Screw-Fastened Cold-Formed Steel-to-Steel Shear Connection Behavior and Models

Sebastien Marc William Corner

Thesis submitted to the faculty of the Virginia Polytechnic Institute and State University in partial fulfillment of the requirements for the degree of

Master of Science

In

Mechanical Engineering

Cristopher D. Moen, Chair

Corina Sandu

Matthew R. Eatherton

December 2nd, 2014

Blacksburg, Virginia

Keywords: self-drilling fastener, cold-formed steel, deformation, limit states

Screw-Fastened Cold-Formed Steel-to-Steel Shear Connection Behavior and Models

Sebastien Marc William Corner

ABSTRACT

This research introduces a proposed model for predicting tilting angle and limit states of single-fastened cold-formed steel-to-steel shear connections. Predictions are validated through an experimental study considering ply configuration and a single Hex #10 -washer head fastener, centered in a 102 mm by 102 mm three boundary window. The fastener tilting angle is captured using an automated, optical non-contact measurement procedure. The results are used to identify cold-formed steel shear connection deformation as load progresses, including tilting, bearing, and combined tilting bearing at the plies and thread tension, shear and bearing fastener failure. Results shows that fastener tilting plays a kinematic affect for the connection. Fastener tilting is predicted in function of ply thickness and fastener pitch. Local ply bending deformation is reported to be the main deformation of the connection during fastener tilting. While fastener bending and shear failure occurred if the fastener does not tilt.

Table of Contents

List of Figures

List of Tables

Chapter 1 Introduction

Light steel-framed structures using cold-formed steel (CFS) as shown in Figure 1-1 are a staple of building construction. Its growing popularity is attributed to lightweight design, low cost in transportation and simple installation (AISI 1999). CFS framing is similar to timber framing using screw fasteners to assemble stud frames. Additionally, CFS has a low risk of fire because it is a non-flammable material with good thermal insulation capacity. Thanks to these advantages, in addition to the demand for low cost construction and budget constraints, CFS structure holds a significant market share. It is estimated that 33% of new low and midrise buildings are made with cold-formed steel today (AISI 1999). This expansion is thanks to the support of organizations such as the American Iron and Steel Institute (AISI) that encourages CFS research including codes and standards development. Research on cold-formed steel has been conducted with synergy from CFS industries and universities under the leadership of the Steel Market Development Institute's construction market program.

It is with this synergy that this research aims to contribute to the state-of-the art in single-fastened cold-formed steel-to-steel shear connections, including *CFS connection kinematics*, (i.e. fastener rotation and translation) and *limit states* (i.e. deformation occurring at peak load) based on steel ply thicknesses combination. CFS connection specifications that will result from this research will contribute toward a new fastener model. This model will be developed through an experimental study based on monotonic loading testing of CFS sheet-to-sheet configuration connected with a single #10 Hex fastener.

Figure 1-1 Example of a CFS light steel framed building at Virginia Tech.

This experimental study contributes to a large cold-formed steel-to-steel shear connection experimental program, which will lay the groundwork for mechanics-based screw fastener load-deformation models. Connection capacity is the focus of most cold-formed steel connection experimental programs in the literature, which is perfectly reasonable for the component level load and resistance factor approaches currently employed in design. A shift to system design is occurring however, which requires not only capacity but also initial stiffness and stiffness degradation with varying load to lead to response equations.

The focus of the research described in this thesis is to study individual steel-to-steel fastener connections and their full load-deformation response, including stiffness degradation as the connection progresses through tilting, bearing, and tearing deformation, with the goal of identifying key kinematics that will guide the large cold-formed steel-to-steel shear connection experimental program to lead to stiffness and capacity prediction and response equations

This large CFS connection experimental program aims to serve as input to 3D building

system modeling and to provide equations for code-based sheathing-to-member deformation compatibility checks. This includes screw fasteners connecting studs to tracks, forming strap braced and sheathed shear walls, and attaching gypsum to interior partitions. These components and their connections define building system behavior, especially lateral drift and seismic performance as demonstrated by recent full scale building tests (Leng et al. 2012).

This large CFS connection experimental program herein is taken from a subset of over 300 single monotonic connection tests conducted with varying t_2/t_1 ply thickness combinations, screw sizes (i.e. #8, #10, #12), screw type (i.e. Hex Washer Head, Truss Head, Flatpan Head, Philips Pancake Head) and employs different practice-oriented specimen boundary conditions – web-to-web (WW, Figure 1-2a), web-to-flange (WF, Figure 1-2) and sheet-to-sheet tests. Connection behavior with two stud cross-sections is explored - 400S162-XX and 600S162-XX, where notation is defined according to the Structural Stud Manufacturers Association (SSMA). The 400 and 600 represent the stud out-to-out widths (4 in. and 6 in., 101.6 mm and 152.4 mm), 162 corresponds to the out-to-out flange width (1.625 in., 41.725mm) having a lip length of 0.5 in (12.7 mm).

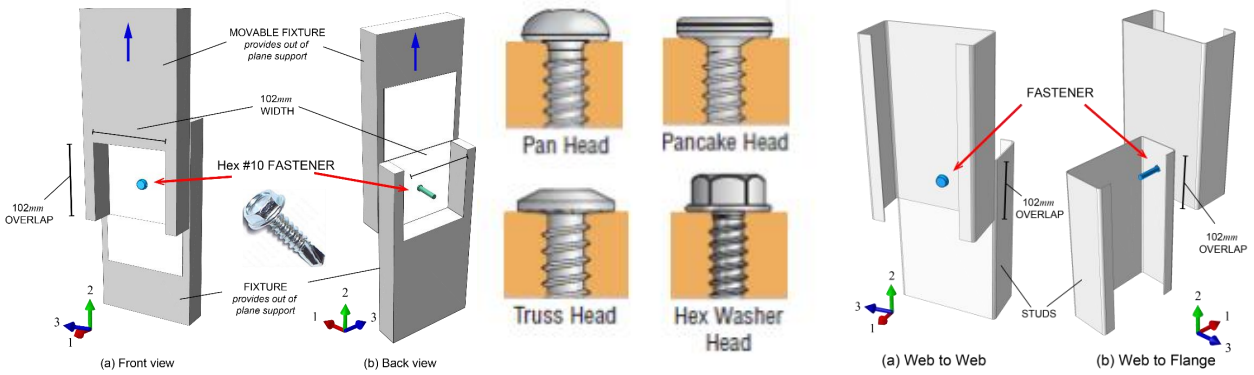

Figure 1-2. Connection test configurations: (a) web-to-web (WW) and (b) web-to-flange (WF) for different screw type (c)

The different stud dimensions and configurations allow for the study of the effect of local boundary conditions on connection response and stiffness. For example, varying from WW to WF can help answer the question, "*Does the connection stiffness increase if it is placed through a narrow flange versus a wide web*?" A hex-washer head self-drilling screw (Simpson Strong-Tie X-Screw series) is used in all tests, with three fastener sizes considered- #8, #10, and #12

The motivation behind this large experimental program comes from new demands from CFS designers and contractors asking for optimized structures that meet structural design standards, performance, safety and cost. As cost is correlated with materials thicknesses and fastener sizes, the results of this experimental study will lead to optimized CFS connections corresponding to improvements in safety and overall screw fastened performance of the connection.

The analysis of the research described in this thesis reports results from sheet-sheet tests using a single #10 Hex fastener and ten different thickness combinations. For each combination, three tests were performed and analyzed. For example, tests with single screw fasteners failing in shear will be reported with the corresponding ply thicknesses.

Screw fastened performance is then related to ultimate fastener displacement δ_f, fastener tilting deformation θ, and fastener load capacity P_{ns}, under monotonic loading P, all related to steel specimen thicknesses t_1 and t_2.

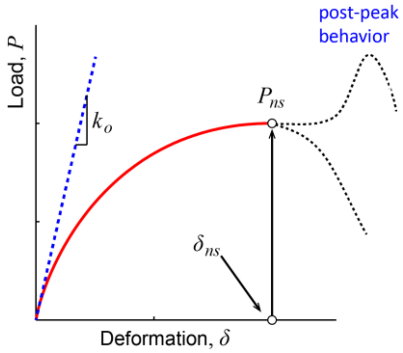

Figure 1-3 Steel-to-steel single shear screw connection load-curve deformation model.

Screw fasteners are easy to install, however their stiffness and strength contributions to the structural system are exceedingly difficult to quantify, this is due to complex kinematics related to, for example, screw head contact and screw-thread interaction. To evaluate screw fastened kinematics, an automated and optical non-contact measurement techniques allows for fastener tracking, i.e., screw rotation and translation and bearing deformation (Figure 1-4) occurring on the connecting members at the fastener location was developed. The deformation occurring at peak load P_f defines the limit state of the connection, which can be seen in a bearing and/ or tilting mode or in shear fastener failure.

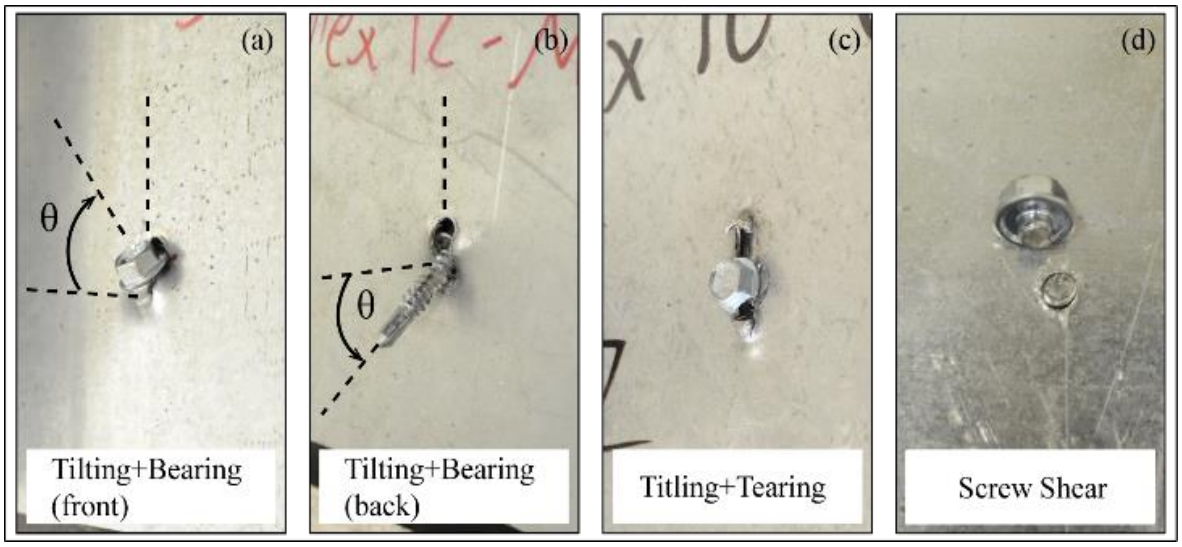

Figure 1-4 Screw fastened deformation, a, b) tilting and bearing , c) ply tearing, d) fastener shear

According to AISI, tilting or/and bearing limit states occurs regarding to the ratio of the bottom ply (i.e. Ply 2) over the top ply (i.e. Ply 1), (i.e. t_2/t_1).

If the ratio $t_2/t_1 \leq 1.0$, tilting or bearing limit state is predicted to occur when the lower capacity value P_{ns} calculated from Equations 1 to 3 predicts the corresponding limit state. The first equation is associated with tilting capacity while the two others are associated with bearing capacity for each respective ply.

$$P_{ns} = 4.2\sqrt{t_2^3 d}\,Fu_2 \quad \text{Eq. 1}$$

$$P_{ns} = 2.7 t_2 d Fu_2 \quad \text{Eq. 2}$$

$$P_{ns} = 2.7 t_1 d Fu_1 \quad \text{Eq. 3}$$

If the ratio t_2/t_1 is in the given range $1.0 < t_2/t_1 < 2.5$, the tilting and bearing limit state is predicted to occur. For this condition, P_{ns} is determined by linear interpolation of the tilting equation (i.e. Eq.1) and bearing equation (minimum of Eq. 2 and 3).

If the ratio $t_2/t_1 \geq 2.5$, bearing limit state is predicted to occur at either Ply 1 or Ply 2. The lower capacity value P_{ns} calculated from Equations 2 to 3 predicts the corresponding limit state.

Fastener shear is predicted with the manufactured screw shear capacity, usually tested with large plies of 6.3 mm.

This thesis is organized based on the following chapter structure. A literature review on cold-formed steel-to-steel connections is presented in Chapter 2. The review describes the theoretical basis for the research based on an evaluative report of previous studies. Chapter 3 presents the proposed screw fastened connection model in predicted fastener tilting and limit states prediction. To validate this proposed model an experimental test study was conducted. The methodology of this experiment program is detailed in Chapter 4, including the optical measurement method and the statistical analysis tool used to determine stiffness degradation. Test results to validate the proposed model is analyzed in Chapter 5. Once validated, the proposed model is compare to AISI model in predicted limit states in Chapter 6. A general conclusion of the analysis of this research and future work is presented in Chapter 7.

Chapter 2 Literature review

Cold-formed steel-to-steel connection tested behavior, both bolted and screw-fastened, are thoroughly documented in the literature. Bolted connected strength limit states are defined by tearing along planes parallel to bolt shear for thin sheet plies, also inclined tearing with material piling up in front of the bolt, transitioning to transverse tearing at the bolt bearing point and then screw shear as ply thickness increases (Winter 1956; Zadanfarrokh and Bryan 1992). Cold-formed steel connection stiffness research resides primarily in bolted connections to improve cold-formed steel truss modeling (Zaharia and Dubina 2006) where both axial and flexural stiffness are empirically derived from tests, and for bolted moment frames (Lim and Nethercot 2004; Uang et al. 2010). Connection strength and stiffness are important for predicting wind and seismic drift.

Connection strength is predicted by the current AISI steel-to-steel screw fastened capacity prediction equations (AISI 2012, Section E4.3). The equations were developed by modifying existing equations (ECCS 1987; British Standards Institution 1987), most notably a change from ply yield strength to ultimate tensile strength that resulted in better predictions confirmed with a compilation study of over 3,500 tests (Peköz 1990; van der Merwe 1987). Strain hardened steels from cold-forming increase fastener capacity and change fastener load-deformation and limit states, for example tearing for high ductility steels may be supplanted by tilting and bearing when the steel thickness is cold-reduced (Daudet and LaBoube 1996).

Screw tilting and bearing strength limit states are defined in the AISI specification based on the plate thickness ratio t_1/t_2, where t_1 is the base metal thickness for the sheet ply in contact with the fastener head and t_2 is the base metal thickness of the adjacent ply typically embedded with at least one fastener thread. Most of these tests were performed by pulling on thin eccentric steel plates (Figure 2-1), which artificially amplifies ply rotation when compared to a typical stud-to-stud or stud-to-track connection. Ply rotation complicates limit state predictions, especially screw shear (Serrette and Peyton 2009).

Figure 2-1 Test set-up for AISI configuration. Ply deflection is allowed and may affect the behavior of the connection. A ply supported test set-up is used in this experimental research to prevent ply deflection.

The tilting limit state is assumed to occur in the AISI capacity equations when $t_2/t_1 \leq 1.0$. Tilting occurs because the shearing force couple resisted by the plies, resulting from the moment in an eccentric single shear connection, causes the fastener hole to elongate in the t_2 ply. As the t_2 ply thickness decreases, the moment arm reduces and the shearing force couple magnitude increases. According to AISI, a tilting failure occurs when a screw, inclined at an angle, pulls through the t_2 ply.

A bearing failure occurs when the concentrated pressure from the fastener on the t_1 or t_2 plies exceeds the steel yield stress causing hole elongation at a constant bearing stress, i.e., the connection shear stiffness decreases to zero. The bearing stress magnitude that causes the stiffness loss varies with fastener distance to an edge. More plate material behind the fastener increases the bearing failure pressure, a phenomenon first documented in bolted cold-formed steel connections (Winter 1956). In the study summarized herein, edge distance on the order of 10 times the fastener diameter is provided and is therefore not a variable.

For thicker plies (97 mils or 2.5 mm) local buckling deformation is minimal in front of a hole and the force can spread and redistribute in the plies. However for thinner plies (33 mils or 0.9 mm) local buckling decreases the ply resistance to bearing. In this case the bearing force is distributed with a tension tie; if the stress in this tension tie exceed the steel ultimate stress, the steel 'rips' in front of the fastener. If both plies are sufficiently thick, then the connection can carry the fastener's shear capacity which is typically determined by each screw manufacturer.

Recent studies show that increasing the number of screws in a connection reduces the strength per screw (Laboube and Sokol 2002). This phenomenon is well documented in reliability theory for a parallel ductile system where the element with the lowest strength redistributes load to its neighbors, driving the system failure (Hendawi and Frangopol 1994). Tests studying combined strength limit states, for example, connections under tension pullout and shear (Francka and LaBoube 2009) demonstrated that screw fastened connection under tension and shear typically failed in a combination of screw pull-out, tilting and sheet bearing.

Screw fastened connections can experience multiple strength limit states at once (Casafont et al. 2006), for example tilting and net section failure and tilting, bearing, and pullout. For simplicity and to concentrate on limit state correlation to load-deformation response, only one fastener is considered in the following test program.

Chapter 3 Screw fastened steel-to-steel model and limit state prediction

This chapter will propose a new model describing screw fastened connection load-deformation response. This model shows the major role played by the head-ply-thread contact in fastener tilting deformation. The proposed model highlights different steel ply thicknesses configuration as a function of the fastener pitch value (Figure 3-1) to predict fastener tilting. Fastener tilting prediction lead to different deformations at the connection. Ply deformation through tilting and bearing, fastener shearing and bending and fastener-thread tension are the main deformations introduced in this model. Thus, fastener tilting prediction will lead to limit state, where the *limit state* refers to the deformation occurring at the connection once the first peak load of the load deformation curve is reached after softening.

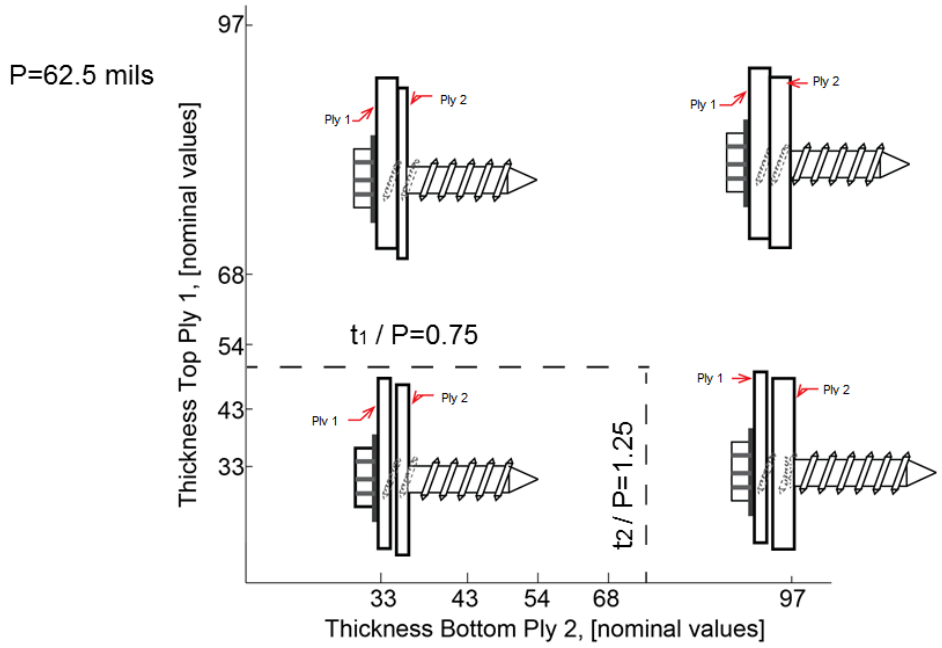

Figure 3-1 Four different schematic representation for cold-formed steel-to-steel connection as a function of Ply 1 and Ply 2 thicknesses. Ply 1 is considered thin if $t_1/P <$ 0.75 and Ply 2 is considered thin if $t_2/P <$ 1.25. Ply thickness combined with the fastener pitch are suggested to be the key parameter in predicted fastener tilting and limit states.

3.1 Proposed model: Head-ply-fastener contact plays a major role in fastener tilting prediction.

For the first configuration with equal ply thickness (Figure 3-1 a), the top Ply 1 and the bottom Ply 2 are locked between the screw head and each thread. Ply 1 is restrained by the head and the first thread, while Ply 2 is clamped between the first and second thread. Using this configuration, a free body diagram is drawn and presented (Figure 3-2, 3-3, 3-4). In the proposed screw fastened model, a shearing force couple results in fastener tilting. The shearing force couple, defined as an applied moment M_c at the centerline between the two plies, is resisted by the head-ply-threads contact forming a resisting moment M_r. Because of the tilting rotation of the fastener, the portion of the fastener in contact with Ply 1 applies a compressive stress F_c on Ply 1 while the fastener shaft in contact with Ply 2 is subjected to tensile force F_t developed by the threads in contact with Ply 2. The thread restrains the fastener from being pulled out, which results in tension on the fastener shaft. Combined, the tensile and compressive forces due to head-ply-thread contact resists the applied shearing force couple moment.

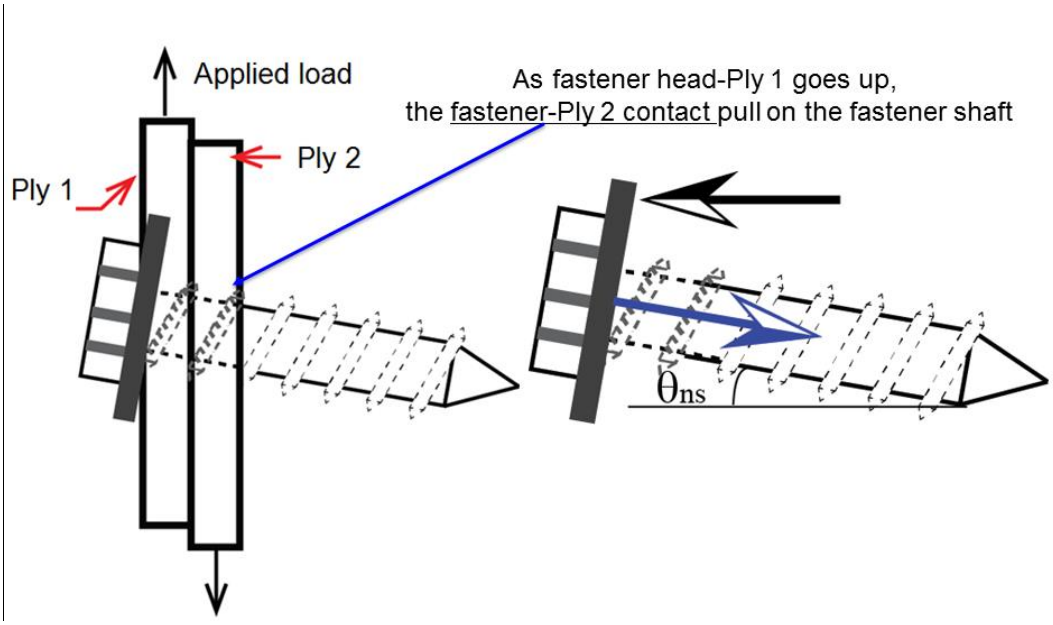

Figure 3-2 Free Body diagram of the proposed screw fastened model while the fastener tilt

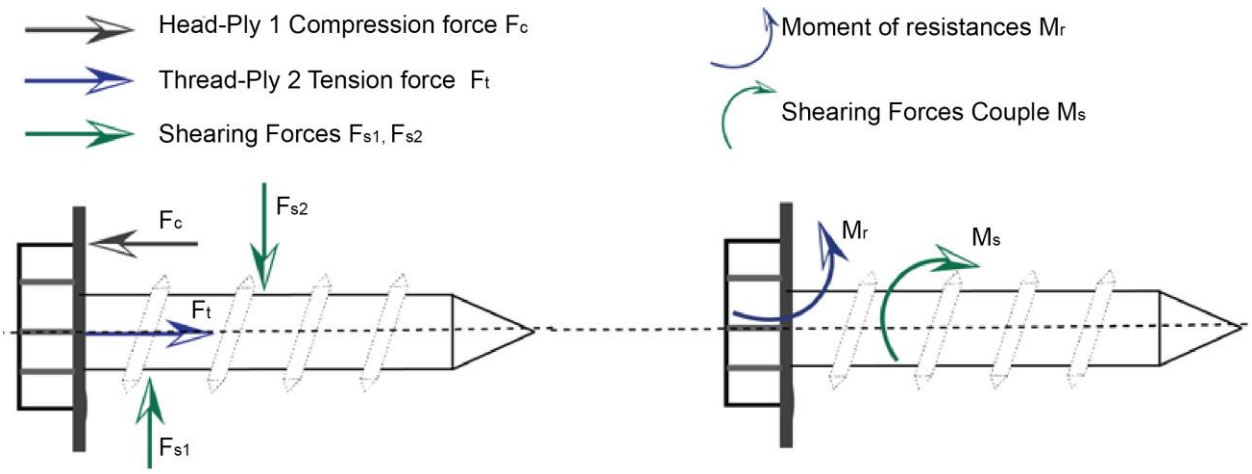

Figure 3-3 Free Body diagram of the proposed screw fastened model

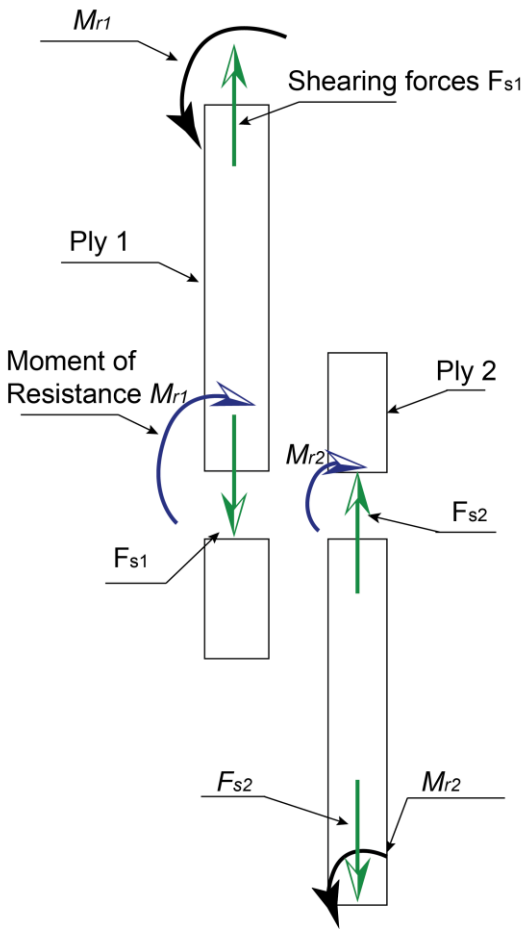

Figure 3-4 Free Body diagram of the proposed screw fastened model at the plies

The resisted moment of the shearing force couple M_r causes a local bending deformation at Ply 1. This deformation allows fastener to tilt. In this proposed model fastener tilting has occurred if the fastener tilting angle at peak load is higher than 10º, ($\theta ns > 10º$). Local bending deformation may also occur at Ply 2. Nevertheless, since the contact surface of the head is approximately 6 times larger than the thread surface for typical screw fasteners, the resisted moment is expected to be higher at Ply 1 compared to Ply 2 for equal thickness plies.

As local bending deformation mostly occurs at Ply 1 and assuming the fastener keeps its rigidity, Ply 2 will tend to deform relative to Ply 1, which should allow fastener tilting. To know how thin Ply 1 and Ply 2 should be to allow local bending deformation or relative ply deformation respectively, it is hypothesized that the fastener pitch should be used as a design variable.

3.2 Proposed model: Fastener tilting prediction related to fastener pitch

This section will highlight fastener tilting prediction according to Ply 1 and Ply 2 thicknesses and the fastener pitch. Ply 1 and Ply 2 differ by their connection with the fastener. A self-drilling fastener is made of threads located at a constant distance *P* from each other's. Ply 1 is located between the head and the first thread, while Ply 2 is between two threads. Typical ply thicknesses should range from 33 to 97 mils (0.83 to 2.46 mm), which is consistent with common industry steel plies. The pitch value *P* for a #10 Hex fastener is equal to 62.5 mils (or 1.5875 mm).

Four different configurations of screw fastened from the proposed model were exposed with their respective ply thicknesses in Figure 3-1. The configuration includes:

a) Ply 1 is thin and Ply 2 is thin ($t_1/P < 0.75$ and $t_2/P < 1.25$, Figure 3-1a),

b) Ply 1 is thick and Ply 2 is thin ($t_1/P > 0.75$ and $t_2/P < 1.25$, Figure 3-1 b),

c) Ply 1 is thin and Ply 2 is thick ($t_1/P < 0.75$ and $t_2/P > 1.25$, Figure 3-1c),

d) Ply 1 is thick and Ply 2 is thick ($t_1/P > 0.75$ and $t_2/P > 1.25$, Figure 3-1d).

Because the head-Ply1 surface contact is greater than the thread-ply contact, the head-Ply 1-thread contact should provide a larger resisted moment than the thread-Ply 2-thread contact. Thus, the head-Ply 1-thread contact should limit faster rotation. The proposed model suggests that Ply 1 should be larger than 75% of the fastener pitch value (i.e. $t_1/P > 0.75$) to be thick enough to prevent fastener tilting. While, a full completely inserted thread into Ply 2 would be required to constrain fastener tilting at Ply 2. The proposed model suggests that Ply 2 should be thicker than 125% of the pitch (i.e. $t_2/P > 1.25$) to constrain fastener rotation. Thus, the proposed model suggests to sort test configurations according to fastener tilting prediction (Figure 3-5).

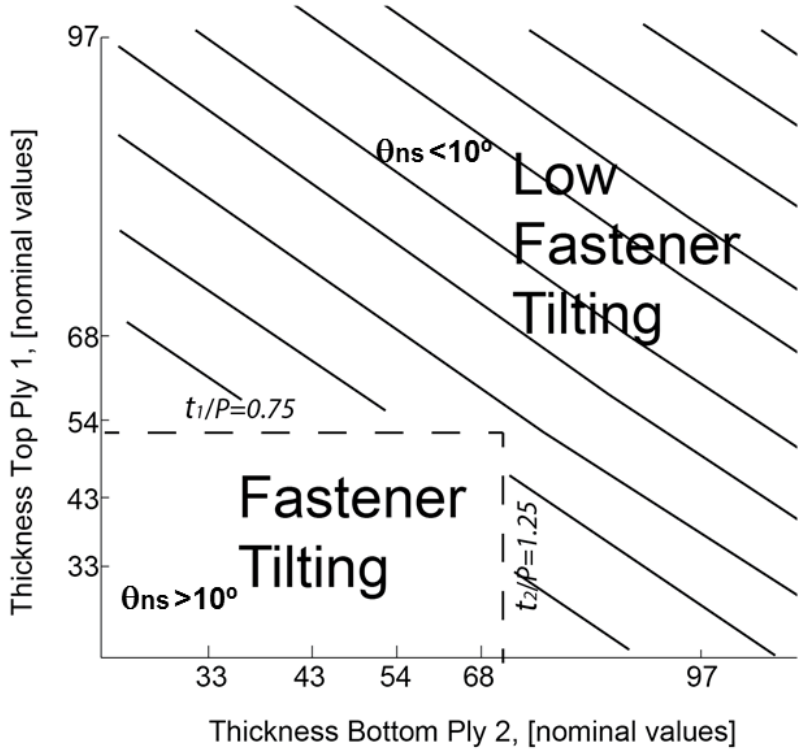

Figure 3-5 Fastener tilting prediction as a function of Ply 1, Ply 2 and fastener pitch *P*. Fastener tilting occur if Ply 1 is thin and Ply 2 is thin ($t_1/P < 0.75$ and $t_2/P < 1.25$)

Given these assumptions, the proposed model now is configured to predict fastener tilting for the four case studies presented in Figure 3-1, as well as the corresponding limit states associated with the prediction.

3.3 Proposed model: Fastener tilting prediction to predict AISI limit states

Fastener tilting prediction lead to different deformations at the connection. The main deformations introduced in this model are ply deformation through tilting and bearing, fastener shearing and bending and fastener-thread tension. The limit states, deformation occurring at peak load, are predicted for the four different configurations of screw fastened (Figure 3-1). The prediction for each configuration includes:

If Ply 1 is thin and Ply 2 is thin ($t_1/P < 0.75$ and $t_2/P < 1.25$, Figure 3-1a), fastener tilting rotation should occur. The proposed model predicts the tilting and bearing deformation as a

predicted limit state for this type of connection. Local bending should occur on Ply 1 and ply deflection on Ply 2, which should cause fastener tilting ($\theta ns > 10^o$). While tilting deformation is occurring, a bearing stress should occur on the cross section of the hole of Ply 2 and Ply 1 resulting from the tensile monotonic applied force transferred by the fastener shaft. In addition, tension force should occur at Ply2-thred contact that prevent the fastener to be pulled out.

If Ply 1 is thick and Ply 2 is thin, ($t_1/P > 0.75$ and $t_2/P < 1.25$, Figure 3-1 b), fastener tilting rotation should not occur. The proposed model predicts bearing and tearing as a limit state. The resisted moment created from the head-Ply 1-thread should prevent the fastener from tilting. As the fastener is estimated to remain horizontal, ($\theta ns < 10^o$), the fastener shaft should bear and tear the thinner ply (Ply 2).

If Ply 1 is thin and Ply 2 is thick, ($t_1/P < 0.75$ and $t_2/P > 1.25$, Figure 3-1c), fastener tilting rotation should not occur. The proposed model predicts bearing and tearing as a limit sate. The resisted moment created from the thread-Ply 2-thread contact should prevent the fastener from tilting, ($\theta ns < 10^o$), which should cause bearing and tearing deformation through Ply 1. Moreover, because Ply 1 is locked between the fastener head and Ply 2, the bearing demand should increase causing material deterioration on Ply 1 unless the fastener fails in shear.

If Ply 1 is thin and Ply 2 is thick, ($t_1/P > 0.75$ and $t_2/P > 1.25$, Figure 3-1d), fastener tilting rotation should not occur. The proposed model suggests fastener shear and bending as a limit state. The head should be restrained on Ply 1, which should cause bending stress at the fastener head because of Ply 2 pushing on the fastener shaft. In addition, Ply 2 should constrain relative rotation with Ply 1 which should cause fastener shear.

This chapter presented a proposed model for fastener tilting and limit state prediction and suggests that the fastener pitch value should be considered as a design factor in predicting fastener tilting. Fastener tilting is predicted if Ply 1 is thin and if Ply 2 is thin (i.e. $t_1/P < 0.75$ and $t_2/P < 1.25$). In configurations that are outside these boundaries, low fastener tilting is predicted. Fastener tilting should play an important role in the limit state prediction and that test configuration need to be sorted according to fastener tilting prediction.

e

Chapter 4 Experimental Study

This research focuses results on load-deformation response of cold-formed steel-to-steel shear connections, with the goal to provide a basis for comparison to the proposed model in Chapter 3 and AISI limit state predictions.

4.1 The experimental study test setup

The experimental study involved the connection of a single #10 hex-washer head, 4.82 mm diameter with thread, centered in the 102 mm by 102 mm sheet window (Figure 4-1) Ply test notation are represented by 400W400-4354, where 400 is the 4in (101.6 mm) width and height of the three edges windows, and the 4354 represents the ply configuration with a bottom 43 Ply 1 and a top 54 Ply 2.

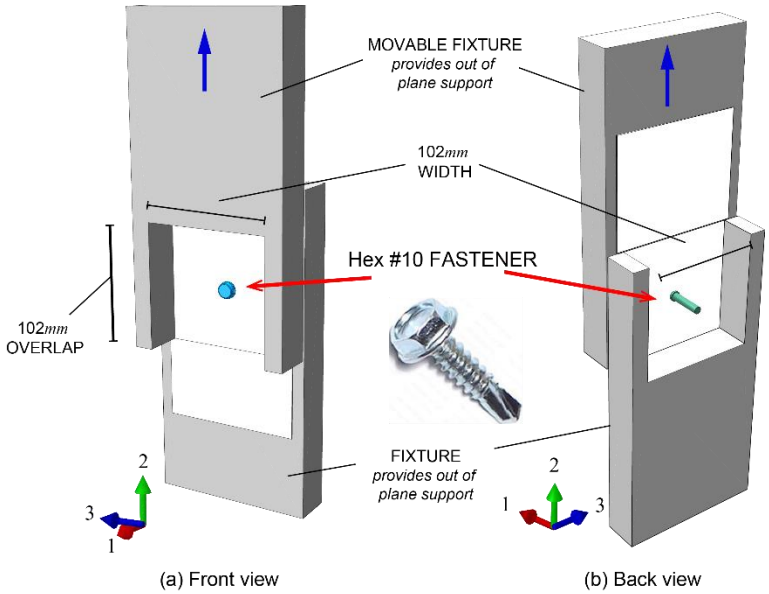

Figure 4-1 Test setup with sheet style boundary conditions where two machined aluminum parts (one bolted to the cross head, one bolted to the testing machine base) creates a 102 by 102 mm square testing area. This setup eliminates specimen curling caused by the moment in the single shear connection.

The ply configuration test set-up was made of a two part custom machined rig, installed on a screw driven MTS Insight 150 Testing System. The upper assembly was fixed into the machine crosshead by a 16 mm rod screw, which supported Ply 1. The upper assembly was composed of two parts – a fixed F block connected and a free-moving rectangular piece. The rectangular piece had an extruded pocket on its top that penetrated the lower vertical inclusion of the fixed F block. This allowed the rectangular piece to slide into the F block and to clamp Ply1 between the rectangular piece and the vertical face of the F block (Figure 4-2)The lower assembly, fixed to the MTS baseplate, supported Ply 2. This lower assembly was made of a triangular block that slides into a fixed base. This sliding motion allowed users to move the lower assembly to change plies quickly. The Hex #10 screw fastened Ply 1 and Ply 2 together with the washer head located on Ply 1 (Figure 4-1)By isolating the fastener, the sheet-to-sheet configuration allows for study of the limit states along with the load connection response. For example, one question that this study will answer is, "*What is the deformation occurring on the connection along the load curve for each ply configuration*?" To identify the deformation along the load curve an optical measurement technique associated with the LVDT was used as discussed in the following section.

4.2 Measurement techniques

A custom machined test setup (Figure 4-2) and a screw driven MTS testing machine were used to perform the monotonic tests. A 150 kN load cell measured applied force and cross head displacement was recorded with an internal LVDT with an accuracy of ± 0.01 mm. The crosshead loading rate is 0.025 mm/sec. An optical measurement device was developed to track the steel specimens and fastener motion, including bearing and tearing, tilting behavior, and relative displacement between the plies.

A rod with two colored circular targets was glued at three locations on a specimen – (*i*) on the fastener head, (*ii*) at 114 mm (4.5 in.) up from the Ply 1 edge, and (*iii*) 25.4 mm (1 in.) down from the Ply 2 edge. Target motion is captured at 1 frame per second with a 35 mm digital SLR camera and then post-processed using Matlab's image processing toolbox to track the movement of the colored targets. For example, the fastener target (*i*) coordinates (C_x, C_y) and (c_x, c_y) as are determined in each picture frame and used to calculate the fastener head rotation θ and translation ($X_f - X_0$, $Y_f - Y_0$). Rod length measurements (L_{rod}) were recorded before each test. Optical measurement accuracy is ±0.50 mm (Haus 2014). The change in vertical displacement between the rod located at (ii) and (iii) is defined as the ply relative displacement. The measurement of the ply vertical relative displacement was compared with the crosshead measurement Δ_c to validate the test.

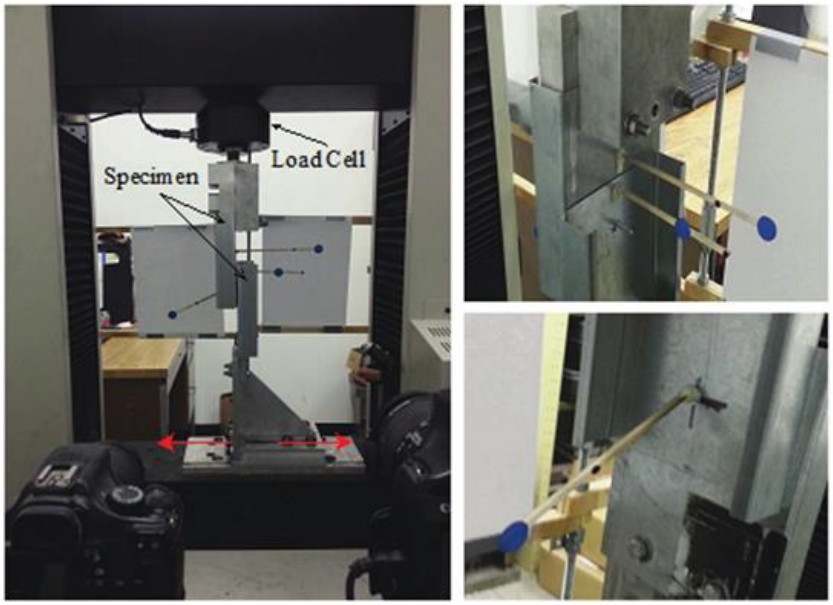

Figure 4-2 Test set-up (a) Front view (left) (b) Right view (right on top) (c) Left view (right on bottom). Location of the rods with two colored circular targets (right) (d)

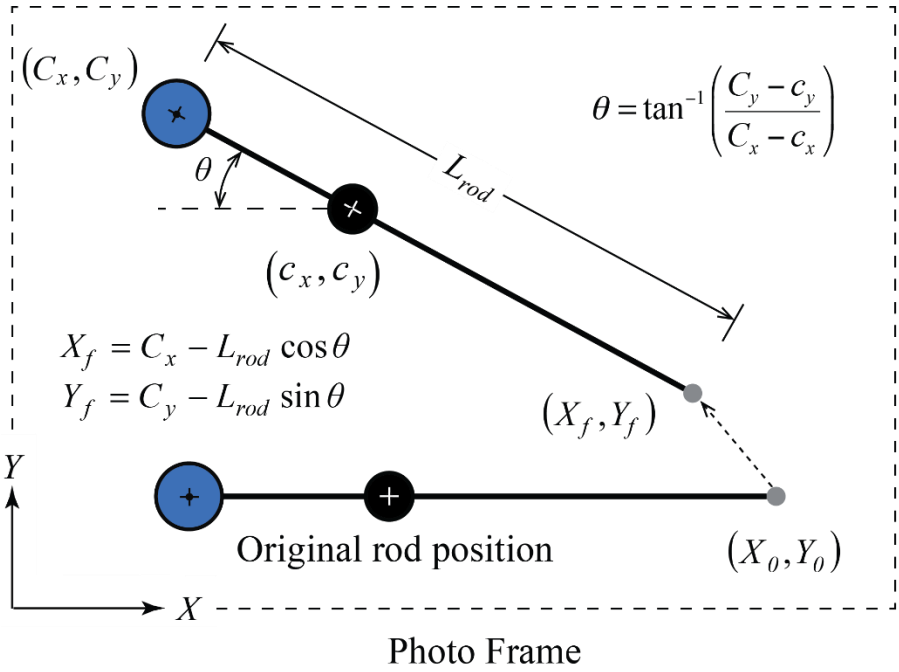

Figure 4-3 Non-contact measurement: the rod is glued on the specimen that tracks its 2D motion

4.3 Testing strategy

The steel-to-steel screw through-fastened connection test matrix with a single #10 Hex fastener is summarized in Table 4-1. Base metal ply thickness combinations were selected to isolate AISI tilting, tilting and bearing, and bearing conditions, as well as three monotonic tests per permutation were performed. The specimen naming notation defines ply 1 and 2 thicknesses in mils (33, 43, 68, and 97) and test number. For example, 3333-1 defines ply 1 and ply 2 as 33 and 33 mils and the test number 1 of 3. Web base metal thickness t_1 and t_2 (i.e., thickness with zinc coating removed) yield stress, F_y, and ultimate strength F_u, were measured for plies 1 and 2 in each specimen. These values are reported in Table 4-1 as an average of two tensile coupons per sheet measured in accordance with ASTM E8M-08 (ASTM 2008).

Table 4-1 Test matrix, measured base metal ply thicknesses t_1 and t_2, yield stress *Fy* and ultimate stress *Fu* from tensile coupons

Ply Configuration	t_1 **[mm]**	t_2 **[mm]**	F_{u1} **[MPa]**	F_{y1} **[MPa]**	F_{u2} **[MPa]**	F_{y2} **[MPa]**
3333	0.880	0.880	446	333	446	333
4343	1.188	1.188	456	337	456	337
9733	2.543	0.868	532	419	445	341
5454	1.406	1.406	533	453	533	453
6843	1.812	1.187	496	392	456	338
4354	1.187	1.402	456	338	531	444
3368	0.885	1.812	444	316	496	392
4368	1.187	1.828	456	338	492	376
4397	1.187	2.549	456	338	524	399
9797	2.553	2.553	523	402	523	402

This chapter presented the experimental study with tests using ply configuration. This configuration helped to investigate the limit states of each connection for each configuration using a self-made optical measurements techniques. Fastener tilting angle were investigated with the optical measurement which helped to explore ply and fastener deformation along the load deformation curves. Results of this investigation are presented in the following section.

4.4 Fastened cold formed steel-to-steel experimental test results

This section presents the fastened cold formed steel-to-steel experimental test results. Screw fastened connection load-deformation response is summarized in Figure 4-4 where *load* is the applied load to Ply 1 (*P*) and the *deformation* is the relative displacement between plies (Δ_c), measured with the crosshead data acquisition. Each curve represents the average load deformation curves for a minimum of 2 tests per combination. A test is named after its ply combination (e.g., 4354, Ply 1 43 mils Ply 2 54 mils). Load deformation curve of each test, including the average curve, are provided in Appendix. Screw fastened connection tilting angle-deformation response is summarized in Figure 4-5. Each curve represents the average angle for

each test and is shown with its respective group, as suggested by the proposed model. All tests are sorted according to the proposed model in predicting fastener tilting. Tests within the "fastener tilting" group are presented as full line curves while tests within the "low fastener tilting" groups are presented as dash lines.

The experimental study presented the test set up configuration which constrains the plies to deform and isolate the fastener in order to allow the deformation to locally deform at the connection. This configuration is different than the test set-up recommended by AISI, where plies are not supported and deformation may spread by ply deformation. The self-made optical measurement allowing faster motion tracking was presented as well as the testing strategy. Results of the experimental study, including load deformation and tilting angle for each test are shown in Figure 4-4 and Figure 4-5. Results are analyzed in chapter 5 to validate the connection proposed model.

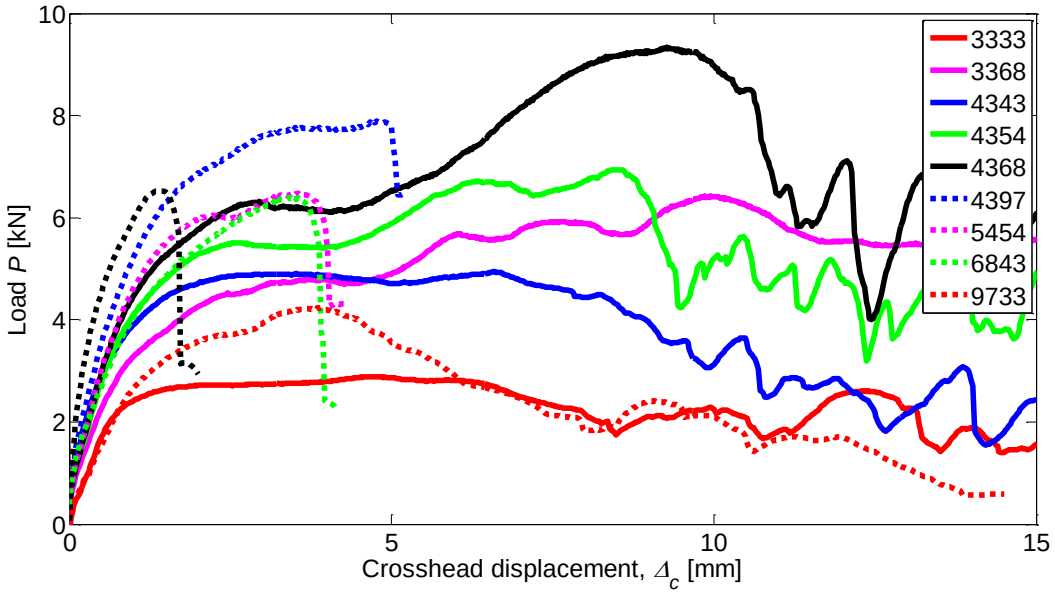

Figure 4-4 Load curves deformation as a function of plies displacement, dashed lines gather tests predicted with "low fastener tilting" while full lines gather tests predicted with " fastener tilting"

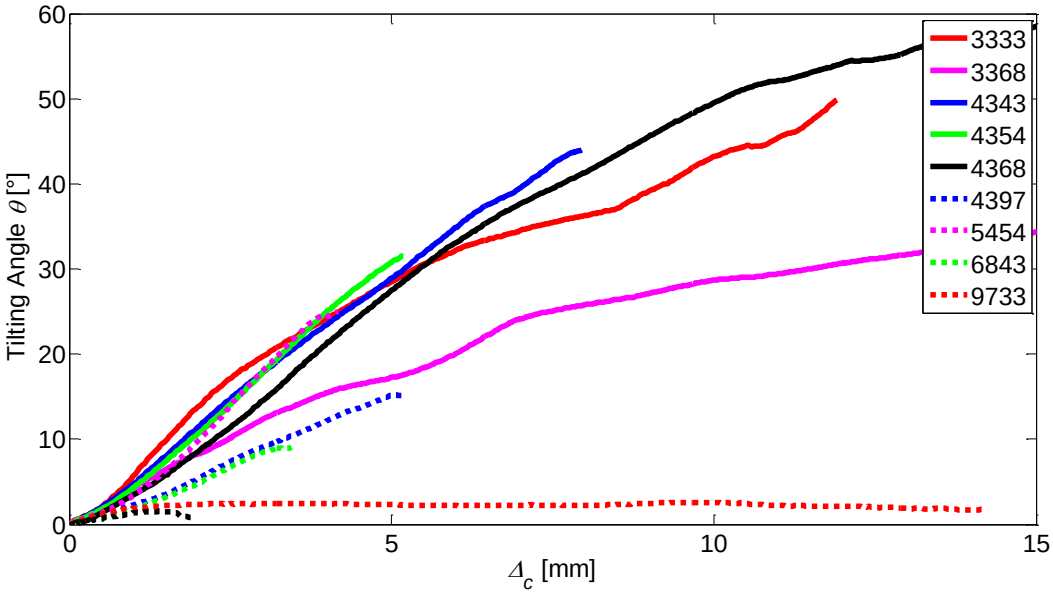

Figure 4-5 Fastener tilting angle as a function of ply displacement, dashed lines gather tests predicted with "low fastener tilting" while full lines gather tests predicted with " fastener tilting"

Chapter 5 Test results to validate the proposed screw fastened model in predicting fastener tilting and limit states

This chapter explores the fastened cold formed steel-to-steel experimental test results presented in Chapter 4 in order to validate the proposed connection model explored in Chapter 3 in predicting fastener tilting and limit states.

The first step in the analysis is to identify fastener tilting deformation for all tests and to determine whether the fastener pitch value can be a design parameter to predict fastener tilting. To determine this assumption tests were sorted into two group: “ fastener tilting” and “low fastener tilting”. According to the proposed model a test was considering low fastener tilting if the fastener angle at peak load was lower than 10 degree. Results and the proposed model are compared through a contour map, where fastener angle is displayed as a function of Ply 1 and Ply 2.

The next step in the analysis is to show that fastener tilting plays a key kinematic in the connection as it contributes to the definition of relevant limit states. Stiffness degradation from initial load to maximum load is studied that enables to link fastener tilting with limit states. Ply deformation occurs at the connection whether the fastener tilted.

Finally, load curve deformation for each test is explored and combined with test pictures analysis of the respective test in order to identify common deformations and validate the proposed model in predicting limit states.

5.1 Test results to validate the proposed screw fastened model in predicting fastener tilting according to the pitch fastener for all tests

Tests results for fastener tilting angle for all tests where presented in chapter 4 where fastener tilting angle were graphed as a function of the crosshead displacement (Figure 4-5). From this plot, two groups of curves are identified as suggested by the proposed model. The group of tests, comprised of 3333, 3368, 4343, 4354, 4368, predicted to be in the "fastener tilting" group, shows similar fastener tilting deformation curves in which the tilting angle at peak load was large ($\theta ns >> 10^{o}$). The next group of tests, comprised of 4397, 5454, 6843, 9733, 9733, predicted to be in the "low fastener tilting" group, shows similar fastener tilting deformation curves in which the tilting angle at peak load was low ($\theta ns < 10^{o}$).

This analysis supports the proposed fastener model, the head-Ply 1-tread contact provides more tilting resistance than the thread-Ply 2-thread contact. It requires a thick Ply 2 to reduce fastener tilting (e.g. 97 Ply 2), while a thinner Ply 1 constrain fastener tilting (e.g. 54 Ply 1). This is due to the fact that a 97 Ply 2 is required to constrain the ply from deflecting, while a 54 Ply prevents local bending of the fastener head into Ply 1.

Based on comparison of the fastener tilting angle curves for each test, a contour map was created to explore fastener tilting angles. A contour map showing initial fastener tilting angle values at peak load, as a function of Ply 1 and Ply 2 thicknesses for a #10 Hex fastener, is presented in (Figure 5-1). A contour map is a map that displays a 3D plot into a 2D map, made of contour lines connecting points with similar data values. Each black dot on the plot represents data points for each ply thickness. The contour map provides a linear interpolation between these lines, helping to identify the trend between the data points. This trend is shown into the color range that goes from light to dark color representing low to large tilting angle respectively.

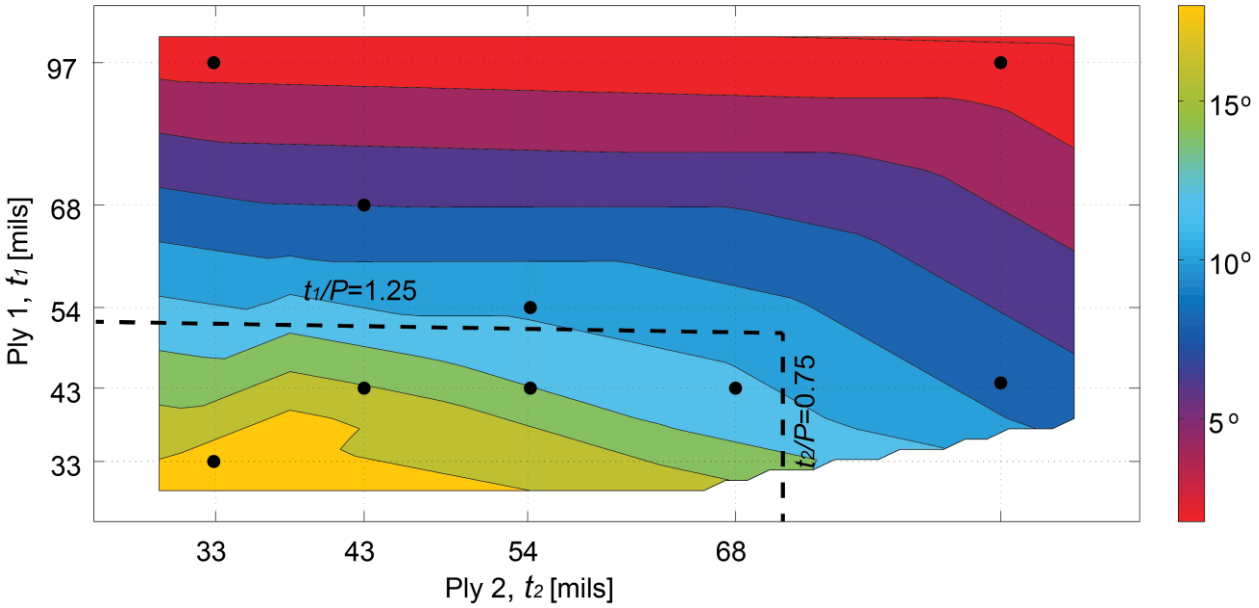

Figure 5-1 Contour map showing the distribution of the fastener's tilting angle at peak load

The crossed black lines differentiate tests experiencing large and low fastener tilting kinematic. They act as a design factor and are associated with the fastener pitch value, whose value for a #10 Hex fastener is 63 mils (1.6 mm). The dashed line crossing the Ply 1 axis is set at 75% of the pitch value while the dashed line crossing the Ply 2 axis is set at 125% of the pitch value, as suggested by the proposed model. This is related to the fact the Head-Ply-thread contact should restrain fastener tilting more than the thread-Ply 2-thread contact. As observed in the contour map, all of the dark color area is located in the left corner of the map and light colors are shown in the other three areas. The analysis based on the contour map validates the proposed model because fastener tilting occurs while t_1 is lower than 75% of the pitch and t_2 is lower than 125% of the pitch (i.e. the dark areas of the map). If the combined Ply 1 and 2 is not located in this range, low tilting is predicted.

In addition to the contour map analysis, an ANOVA statistical analysis of fastener tilting angle for each group of tests is studied. Tests including into the "fastener tilting angle" group (Table 5-1 a) have a group mean value for tilting angle of 17.4 º with a standard of deviation of 2.1 7 º. As the tilting angle mean for each test of the "fastener tilting angle" group is closed by one standard of deviation to the tilting angle mean of the group, the statistical analysis validates tilting prediction for these tests. Moreover, the statistical analysis validates the tilting angle limit of θns=10º used to predict if fastener tilting occurs for a given test. This is identified by the fact that 10º is at three time the standard of deviation from the fastener tilting mean value of the "fastener tilting angle" group. Thus, tests with a fastener tilting angle mean value lower than 10º are rejected to be in the tilting group. The probability that the test mean is considered to be equal to the fattener tilting mean value of the tilting group is less than 5%. Therefore, prediction for tests into the "low fastener tilting" group is validated (Table 5-1 b).

Table 5-1 Tilting angle mean value at peak load a) for tests into the " fastener tilting " group and b) for tests into the" low fastener tilting " group.

Tests	Angle θns (degree)
3333	19.5
4343	18.8
4354	17.1
4368	13.9
3368	17.7
Mean	17.4
Std	2.17

Tests	Angle θns (degree)
5454	13
6843	9.3
9797	1.5
9733	2.3
4397	9.2
Mean	7.06
Std	4.96

This section has demonstrated that fastener tilting kinematic can be predicted according to the fastener pitch and ply thicknesses, as suggested by the proposed fastener model. The next section will relate fastener tilting to the limit state predictions.

5.2 *Fastener tilting: a key kinematic in Screw-Fastened Cold-Formed Steel-to-Steel Shear Connection Behavior*

The proposed model identified fastener tilting as a key kinematic in screw-fastened cold-formed steel-to-steel shear connection Behavior. To validate this assumption, the analysis is investigated the load deformation curves associated to tests included in the "tilting group" (Figure 5-2) and shows that fastener tilting is a key kinematic because these tests share a similar tilting and bearing limit state, as suggested by the proposed model. Fastener tilting linked to predicted limit states, is determined by studying stiffness degradation on the load curve associated with deformation occurring at the connection using the 4368 test as example.

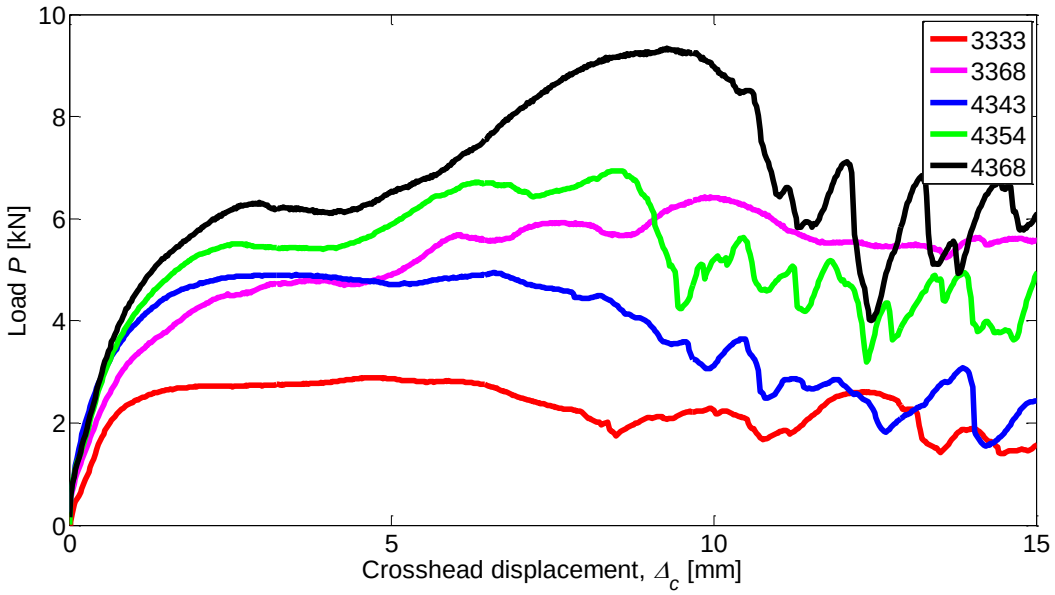

Figure 5-2 Load curves deformation for tests included in the" fastener tilting" group

A self-made curve fitting generated by linear lines (Figure 5-3) is introduced in this thesis to determine stiffness degradation on a load curve. The methodology of this approach is based of statistical analysis tool described in Appendix A. One assumption of this statistical study was that the secant derivative of the deformation load curve from initial value to the first peak load is normally distributed. The first line is a regression line of the data from the higher tail of the

distribution, where the stiffness secant values are much higher than the mean value of the secant stiffness distribution. While the second line has stiffness closely equivalent to the mean value of the distribution. The green and red lines are linear regressions from the peak load to the maximum strength point. These linear fits determine that the connection experienced stiffness degradation along the load deformation curve resulting from a change of deformation that goes from tilting deformation (i.e. local bending deformation into plies) to tilting and bearing limit state.

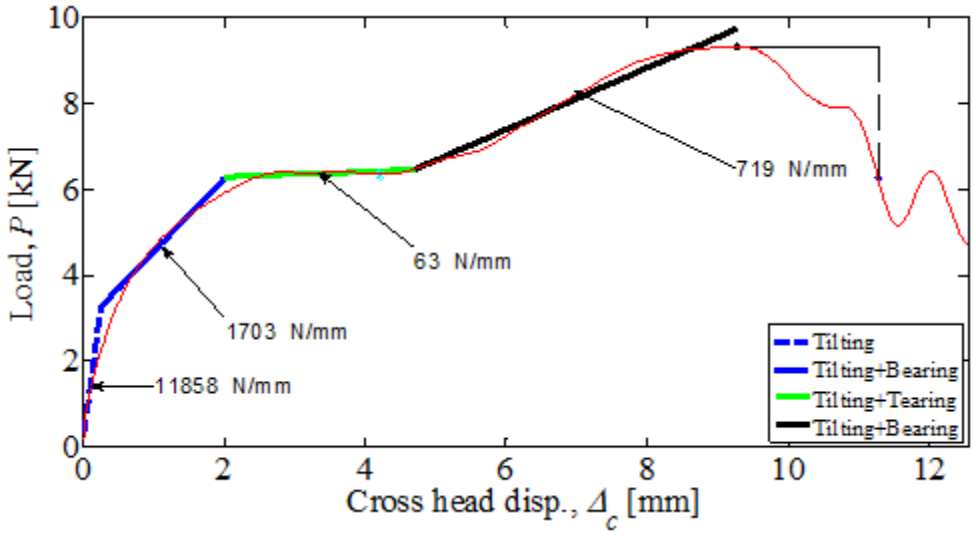

Figure 5-3 Load curve deformation with curve linear fitting, showing stiffness degradation, for the given metal specimen thickness combination 4368 t_1=43 and t_2=68.

For tests gathering in the "Tilting group" such as the 4368 tests, initial deformation goes through tilting, represented by the first blue dashed line. While the second blue line identifies the fact that tilting is associated with bearing. During the tilting initial stage, the load was not large enough to create bearing deformation. The head started to locally bend Ply 1 allowing fastener rotation. The second blue line shows the connection tilted and starts to bear. The shearing force couple causing fastener tilting, implied a bearing demand at each ply, which generated hole elongation and caused stiffness degradation represented by the intersection of the two first blue

lines. A bearing limit state occurs when the concentrated pressure from the fastener on Ply 1 or 2 exceeds the steel yield stress causing hole elongation at a constant bearing stress, i.e., the connection shear stiffness decreases to zero, represented by the intersection of the blue and green line. Since tilting is still occurring during this stage, the limit state experienced by the 4368 test is bearing and tilting.

Fastener tilting linked to tilting and bearing limit state by stiffness degradation can be reported through all the tests included in the "tilting group". Load deformation for each test is graphed into Figure 5-2. The graph shows similar load deformation from initial load to peak load for all the five tests resulted from tilting and bearing deformation. This deformation is highlighted into the next investigation, where photos for each ply configuration after testing are presented. The analysis explores pictures made after testing for each test of the "tilting group". This approach aims to investigate deformations occurring at the connection and correlate them with the load deformation study in order to validate the proposed model in predicting tilting and limit state for test included in the "fastener tilting" group.

5.3 Test results to validate the proposed screw fastened model in predicted limit states for tests within the predicted "fastener tilting" group

The analysis is now shifting to the test pictures investigation to validate the proposed model in predicting limit states for the "tilting group". Although tests experience the same bearing and tilting limit state, highlighted in this analysis, the "tilting group" can be sorted into three different subgroups as the post peak deformation is notably different. The first subgroup gathers the 4343 and 3333 tests, with post peak bearing deformation. The second subgroup gathers the 4368 and 4354 tests, with post peak hardening results from bearing and material piling in the 68 and 54 mil Ply 2. The last subgroup gathers 3368 tests, with post peak tearing

deformation.

Beginning with the first subgroup, the 3333 and 4343 tests are tilting dominated with bearing hole consistent with the proposed model (Figure 5-4, Figure 5-5). The fastener head penetrated the ply, allowing fastener tilting rotation. The average tilting angle degrees at peak load was θ=19.5 degrees for the 3333 test, where peak load is defined for each test as the first local maximum load after curve softening. The increased ply thickness in the 4343 tests has a minimal effect on tilting deformation (θ=18.8 degrees) compared to the 3333 tests (θ=19.5 degrees). The 4343 test (Figure 5-5) experienced similar deformation as the 3333 test (Figure 5-4). The fastener head penetrated the ply due to local bending deformation, which allowed fastener tilting.

However, the increased thickness from 4343 to 4354 boosts connection capacity (or peak load) by 75% (P_{nst}=4924 N) when compared to the 3333 tests (P_{ns}=2806 N) (Figure 5-2). The higher capacity comes from the tension force of the fastener thread with Ply 2. During fastener tilting, the monotonic load was transferred to the fastener by shear and tension to the threads in contact with the Ply 2. The thread-Ply 2 tension prevented the fastener from pulling out, therefore, increased the load capacity of the connection as Ply 2 thickness increased. The increase of the tensile force as Ply 2 is thicker is seen at the damage of the threads caused by tensile forces for the 4343 test (Figure 5-5 b).

As the tension force increased with the load, the thread in contact with Ply 2 damaged and the hole at each ply elongated, which caused the load to peak. Then a bearing failure occurred, the load remained constant during a large crosshead displacement (Figure 5-2). The hole elongated at constant stress until the thread in Ply 2 completely damaged (Figure 5-5 b) or the thread went through the hole because of material deterioration at the hole (Figure 5-4).

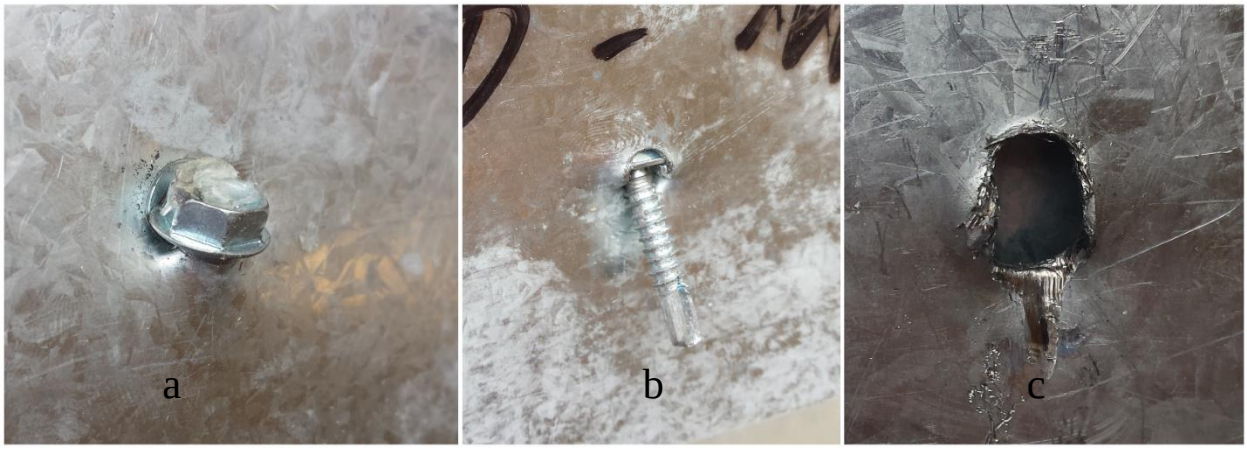

Figure 5-4 Photo showing 3333 test a) Head in Ply 1, b) fastener shaft in Ply 1, c) bored hole in Ply 2

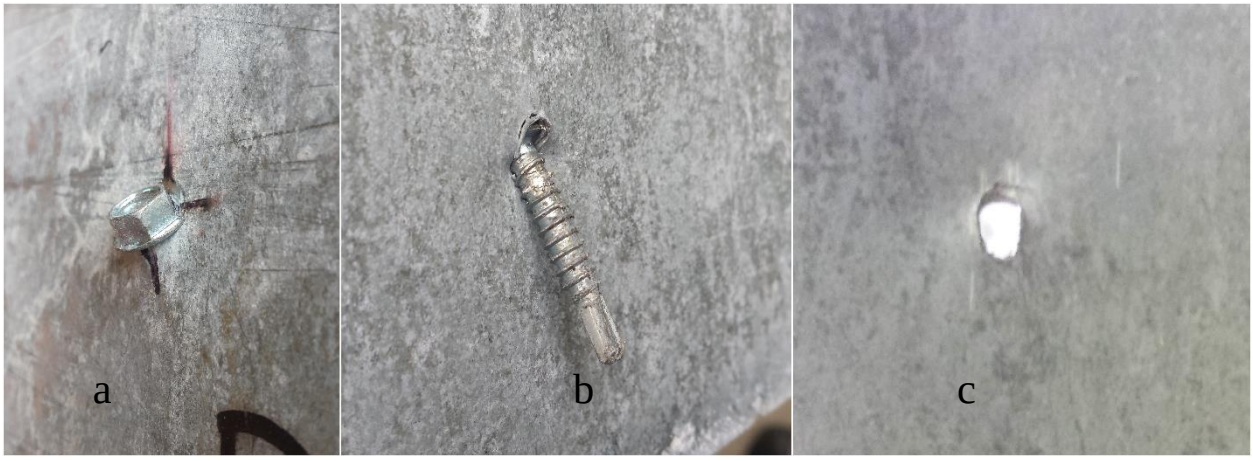

Figure 5-5 Photo showing 4343 test a) Head in Ply 1, b) fastener shaft in Ply 1, c) bored hole in Ply 2

The second subgroup gathering the 4368 and 4354 tests are tilting dominated with bearing hole consistent with the proposed model (Figure 5-6, Figure 5-7). The average tilting angle degrees at peak load was θ=17.1 degrees for the 4354 test and θ=13.9 degrees for the 4368.

These tests presents the advantage of having the largest maximum load. The increased thickness of Ply 2 from 4343 to 4354 boosts connection capacity at peak load by 11% (P_{nst}=5502 N) and boosts connection maximum load by 27% (P_{max}=6265 N) when compared to the 4343 tests (P_{max}=P_{ns}=4924 N). The increased thickness from 4343 to 4368 boosts connection capacity

by 30% (P_{nst}=6419 N) and boosts connection maximum load by 68% (P_{max}=8265 N) when compared to the 4343 tests (P_{ns}=4924N) The higher capacity comes from the post peak material hardening in Ply 2. Before reaching peak load and during the bearing and tilting phase, material was accumulated and wrinkled on the fastener (Figure 5-6, 5-12 c). This accumulated material increased thread tension at Ply 2, which prevented the fastener from pulling out, therefore, increased the maximum load capacity. At the peak load value, material yielding was reached and a part of the accumulated material around the fastener was deteriorated at a constant load, which resulted in a flat load deformation curve (represented by the green line in (Figure 5-3). The remaining post peak material hardening causes stiffness growth (represented by the red line in Figure 5-3). The fastener was restricted until it started to pull out in a combined tension-shear mode, causing thread degradation (Figure 5-6, 5-12 b).

The fastener's connection failed because the thread in Ply 2 pulled out through the hole, which caused a significant drop in the load. Failure occurred at a load of 9 kN and around 8 mm crosshead displacement, which represents 165% of the screw diameter. Thus, the results confirm the advantage of having a very high maximum load but also having a large deformation capacity.

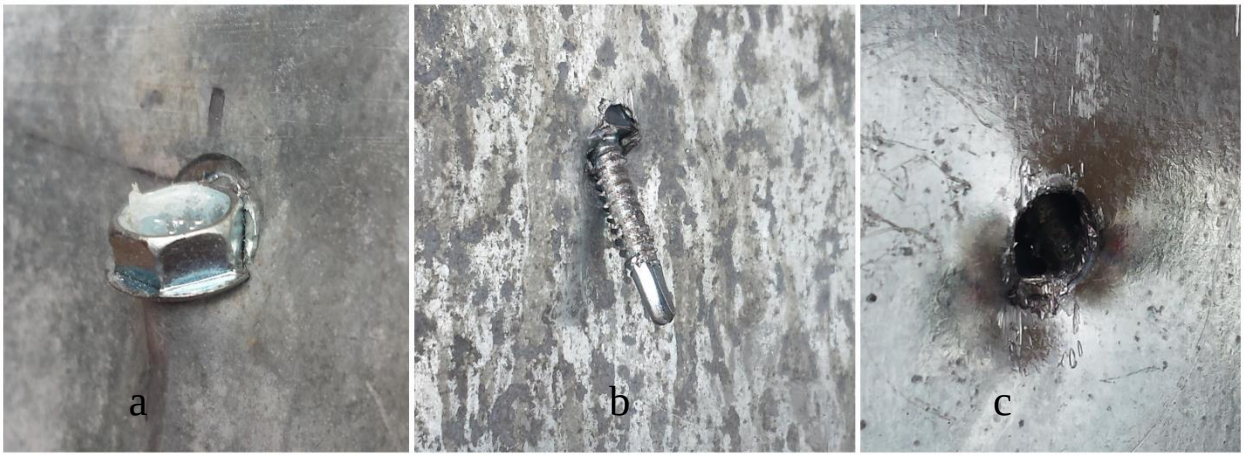

Figure 5-6 Photo showing 4354 test a) Head in Ply 1, b) fastener shaft in Ply 1, c) bored hole in Ply 2

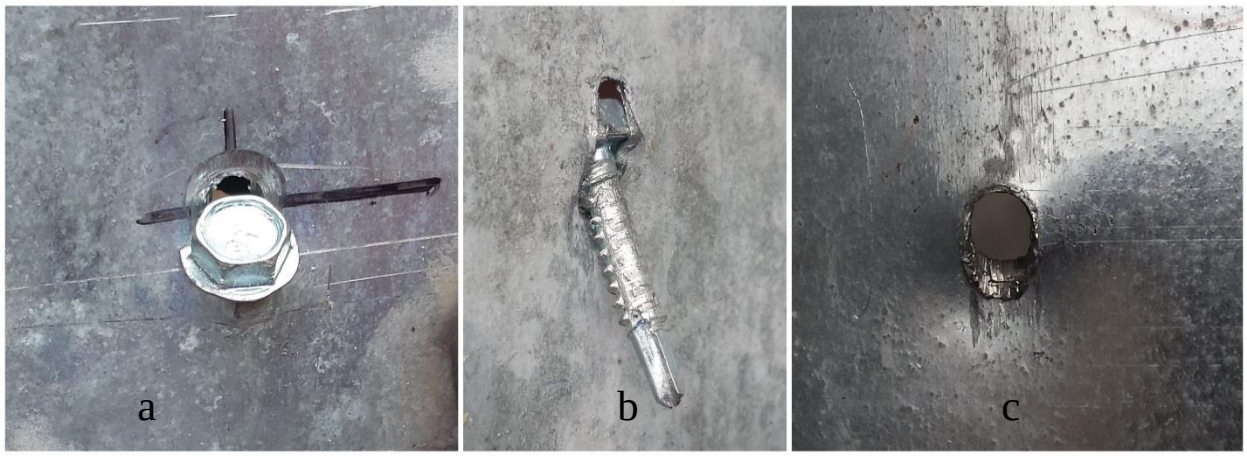

Figure 5-7 Photo showing 4368 test a) Head in Ply 1, b) fastener shaft in Ply 1, c) bored hole in Ply 2

The third subgroup (i.e. 3368 tests) are also tilting dominated with bearing hole consistent with the proposed model. The average tilting angle degrees at peak load was θ=17.7 degrees. The increased Ply 2 in the 3368 tests has a minimal effect on tilting deformation (θ=17.7 degrees) compared to the 3333 tests (θ=19.5 degrees).

However, the 3368 tests experienced post peak load with material degradation through tearing. Tearing occurs when hole elongation endures stressed at a constant bearing pressure during a prolonged period of time, which causes material degeneration. While the 3333 and 4343 configurations experienced tilting at Ply 1 and bearing at Ply 2, the 3368 configuration experienced tilting at Ply2 and bearing in Ply 1, as predicted by the proposed model (Figure 5-8). While the fastener tilted because of Ply 2 deflection, the bearing stress increased on Ply 1, which caused hole elongation and deterioration. The bearing and tearing deformation occurred several time causing load undulation until the fastener reached the edge of the ply (Figure 5-8 a). The accumulated steal material during the bearing phase increased connection capacity, following with deterioration of the accumulated steal causing load dropped.

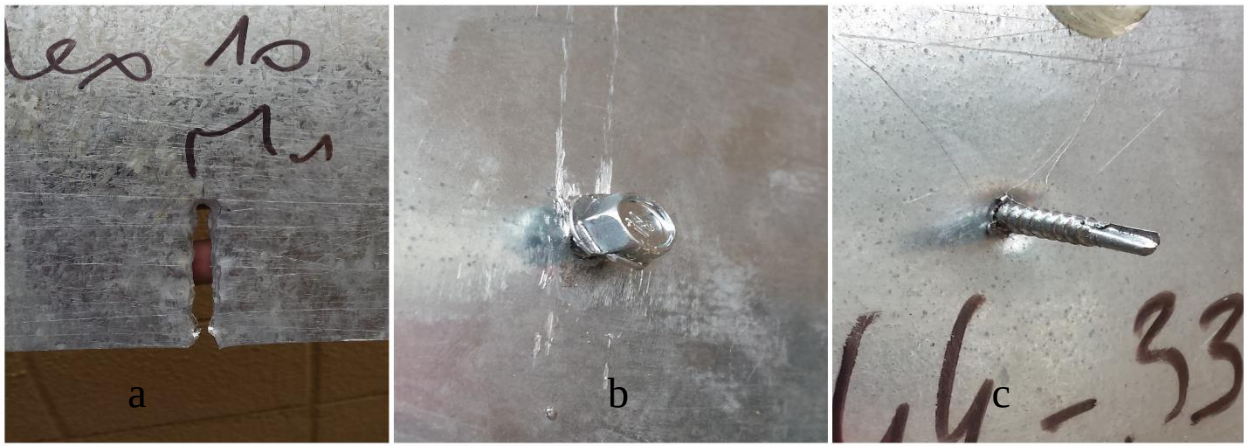

Figure 5-8 Photo showing 3368 a)Tore hole in Ply 1, b) Head in Ply 2, c) fastener in Ply 2

The proposed model in predicting tilting deformation causing bearing and tilting limit state was validated. In addition, the analysis show that Ply 2 plays an important role in increasing connection capacity and confirms that Ply 1 governs fastener tilting. The experimental analysis will explore limit state for tests experiencing low fastener tilting deformation.

.

5.4 Test results to validate the proposed screw fastened model in predicted limit states for tests within the predicted " low fastener tilting" group

Fastener tilting was determined to be a key kinematic in screw-fastened cold-formed steel-to-steel shear connection. The limit states associated with tests included with "fastener tilting" were validated. In this section, the analysis validates limit states associated with tests included with "low fastener tilting", by studying the load deformation curves and their associated testing pictures. Although tests experience the same bearing and tilting limit state, highlighted in this analysis, the "tilting group" can be sorted into three different subgroups as the post peak deformation is notably different. The proposed model suggested to sort the "low faster tilting" group in three subgroups. The first group gather tests with quasi equivalent plies (i.e. 5454, 6843, and 9797), the second group is composed of Ply 1 < < Ply 2 (i.e. 4397) and the third group is composed of Ply 1 >> Ply 2 (i.e. 9733).

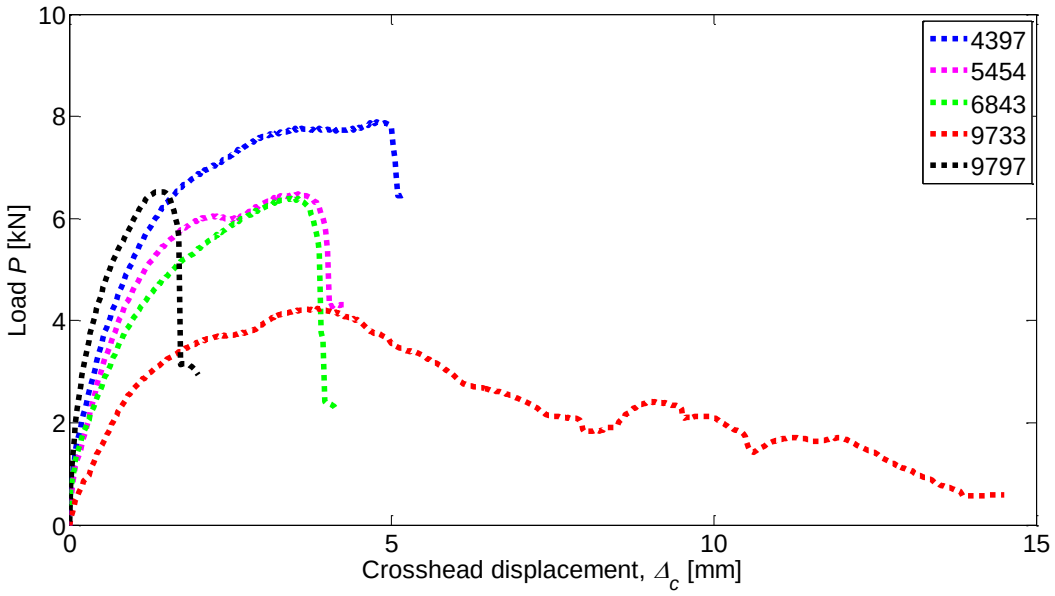

Figure 5-9 Load curves deformation for tests experiencing dominant fastener tilting

Beginning with the first subgroup, the 5454, 6843 and 9733 tests are low fastener tilting resulted to fastener shear and bending failure. For the 5454 configuration Figure 5-10), the average tilting angle degrees at peak load was θ=13 degrees. Fastener tilting angle was similar to 5454 compared to the 4368 tests (θ=13.9 degrees). The reason of this measurement is that the fastened head, especially the washer, deformed. This deformation caused the measurement reading to be as high as if the fastener tilted, while pictures from Figure 5-10 shown that fastener shaft tilting was low. Ply local deformation at Ply 1 did not occur. As the propose model predicted, fastener tilting was restrained due to the head-Ply 1-thread contact (i.e. Ply 1 was thick enough to prevent local bending). The moment concentrated at the Ply 1 head contact increases, causing bending of the fastener shaft and a brittle failure (Figure 5-10) at peak load as the fastener shaft breaks at the screw head.

Figure 5-10 Photo showing 5454 test a) Head in Ply 1, b) Broken fastener in Ply 1, c) Broken fastener in Ply 2

Similar as the 5454 configuration, the 6843 failed in a combination of shear and bending of the fastener as suggested by the proposed model. Although having different ply thickness, the 68 Ply 1 prevents the fastener from large tilting (Figure 4-5). The average tilting angle degrees at peak load was θ=9.3 degrees. This low tilting angle was predicted by the proposed model while AISI model predicted tilting deformation as Ply 2 is thicker than Ply 1 (t_2=43 / t_1=68 <1). The fastener shaft remained horizontal, causing an increase of bearing stress on Ply 2. This bearing stress applied perpendicular forces to the fastener shaft, which caused fastener bending and shearing.

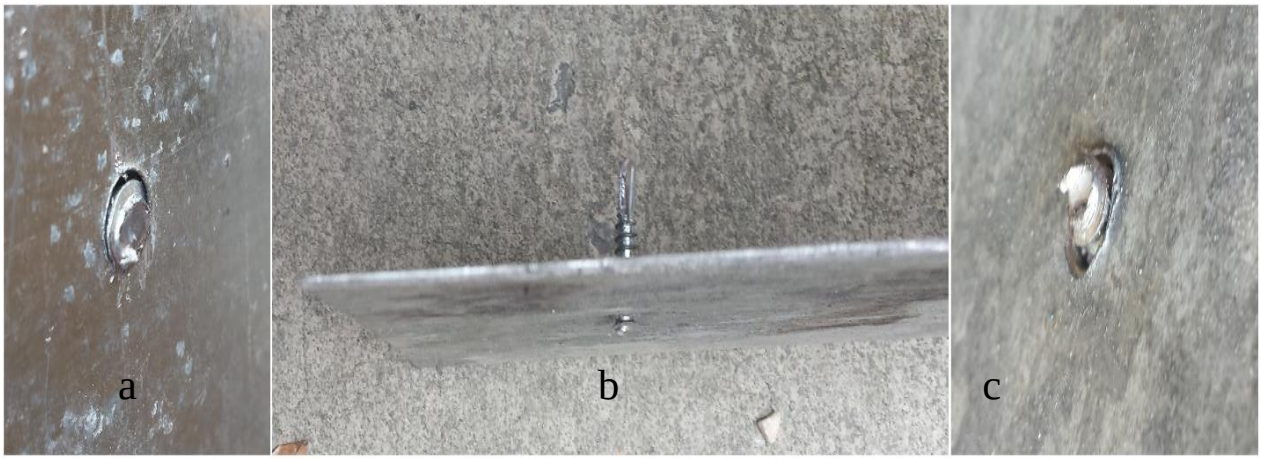

Figure 5-11 Photo showing 6843 test a) Broken fastener in Ply 2 b) Broken fastener in Ply 2 c) Broken fastener in Ply 2

A brittle failure test (Figure 5-11) at a peak load of 6.2 kN occurred. This failure and the peak load were the same as the 5454 test (Figure 5-9).

As the next step in the analysis, the 9797 test was used to estimate the fastener shear and bending failure capacity. The average tilting angle degrees at peak load was θ=1.5 degrees. Manufacturer screw shear capacities (P_{ss} in AISI S100-12) are usually tested with 283 mil (6.3 mm) plies. A peak load of 8.2kN is provided as the shear failure point for the fastener. The observed peak load reached a value of 6.2 kN, which corresponds to the observed value for the 6843 and 5454 tests. This observed peak load is lower than the manufacture peak load because the screw fails by a combination of screw shear and bending (Figure 5-12) in the 9797 test, which does not occur in manufacturer's tests.

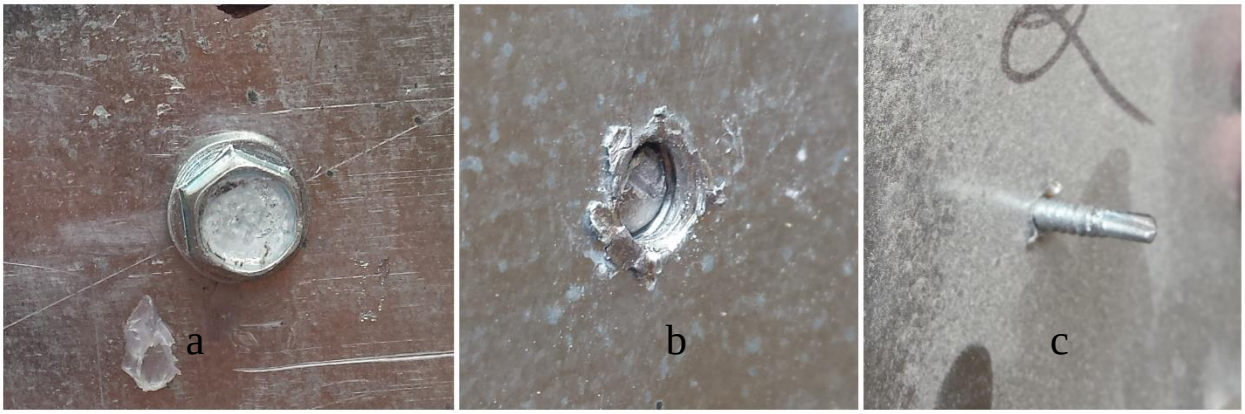

Figure 5-12 Photo showing 9797 test a) Head in Ply 1, b) Bending and shear fastener failure at the head, in Ply 1, c) fastener remains in Ply 2

The next subgroup composed of the 9733 test presents low fastener tilting combined with bearing dominant at Ply 2, as suggested by the proposed model. The average tilting angle degrees at peak load was θ=2.3 degrees Ply 1 constrained the fastener from tilting, which caused the fastener shaft to remain horizontal (Figure 5-13 a). The analysis shown that for this type of configuration in which Ply 1 is much thicker than Ply 2, the tilting limit state predicted by the

AISI model was inconsistent with observations. The horizontal shaft provided a full bearing stress on the hole cross section of the thin Ply 2, leading to a dominant bearing limit state with a peak load around 4kN (Figure 4-4). The peak load is located between the 3333 and 4343 configuration showing a low connection strength due to the low bearing capacity of Ply 2. The load drop at peak load because the weak tension force between the thread with Ply 2 due to hole elongation through tearing. As the hole elongated, post peak material hardening at Ply 2 build-up (Figure 5-13 b). The bearing stress increased and applied perpendicular forces to the fastener shaft, which caused fastener bending and brittle failure test (Figure 5-13 a).

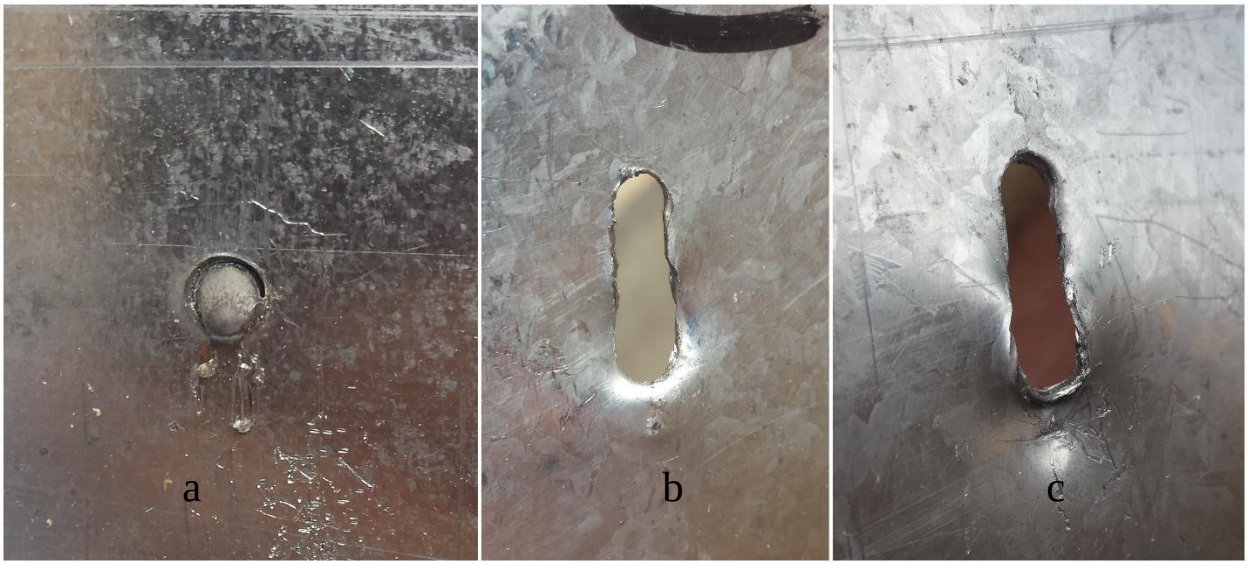

Figure 5-13 Photo showing 9733 test a) Fastener bending, b) Tore Ply 2, c) Tore Ply 2

As the next step in the analysis, the subgroup composed of the 4397 test experienced a dominant bearing limit state at Ply 1 combined with low fastener tilting as suggest by the proposed model. The average tilting angle degrees at peak load was θ=9.2 degrees. Opposite configuration than 9733, the 4397 has Ply 2 much thicker than Ply 1.

The 4397 configuration experienced a dominant bearing limit state at Ply 1 because Ply 2 constrained fastener tilting. As suggested by the proposed model, a thick Ply 2 prevented the

fastener from ply deflection. The fastener remained horizontal and bore the thin Ply 1. This constrain made the connection very stiff (Figure 4-4) compare to other configuration. This connection worked as a rigid body in which initial deformation went through bearing at Ply 1 only. Material piling around the head occurred during hole elongation. The stress generated at the head caused the connection to fail in pure fastener shear at 8kN, consistent with the manufacturer screw shear capacity. Shearing failure is shown by the shear cross sectional area of the fastener, as well as by the intense deformation of the plies due to shear friction (Figure 5-14b).

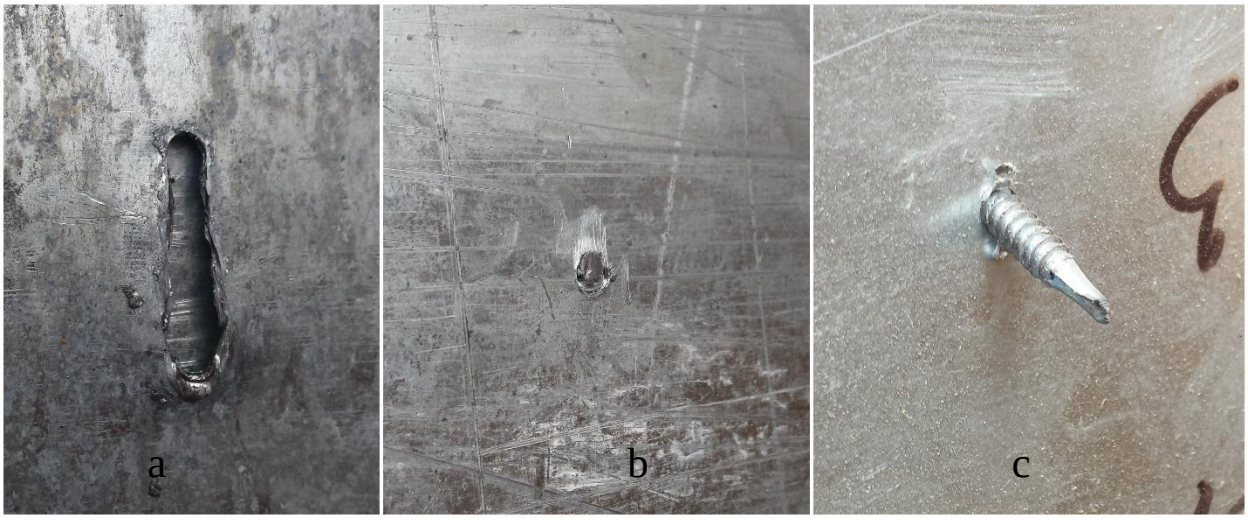

Figure 5-14 Photo showing 4397 test a)Tore hole at Ply 1, b) Shear failure at the fastener head in Ply 2, c) fastener in Ply 2 after failure

The analysis shown dominant bearing limit state for large different ply thickness configurations, and determined fastener bending failure for the 9733 test and fastener shear failure for the 4397 test. Therefore, the analysis shown that if the ply configuration constrains fastener tilting and if each ply of the configuration is thick enough to answer to the bearing demand, the connection limit state will be a combination of shear and bending of the fastener (e.g., 6843, 5454, 9797).

5.5 *Conclusion of the analysis*

Experimental results (

Table 5-2,), using a single #10 Hex fastener and plies configuration validated the proposed screw fastened model for predicting fastener tilting and connection limit states.

Table 5-2 Summary of the experimental results

Tests	Experimental Results				
	Fastener Tilt.	Deformation at Ply 1	Deformation at Ply 2	Limit State	Failure
3333	Yes	T+B	T+B	T+B	Tearing /pull out
4343	Yes	T+B	T+B	T+B	Tension/pull out
4354	Yes	T+B	Deflect.	T+B	Tension/pull out
4368	Yes	T+B	Deflect.	T+B	Tension/pull out
3368	Yes	T+B	Deflect.	T+B	Ply 1 Tore
5454	No			Bend. and Shear	Bend. and Shear
6843	No			Bend. and Shear	Bend. and Shear
9797	No			Bend. and Shear	Bend. and Shear
9733	No		Bearing	Bear. dom. Ply2	Bending
4397	No	Bearing		Bear. dom. Ply1	shear

T+B: Tilting and Bearing; Bend. and Shear: Fastener bending and shear

Results show that fastener tilting, causing by the shearing force couple, is a key kinematic in screw-fastened cold-formed steel-to-steel shear connection. The kinematic effect is associated with local bending deformation of the fastener head into Ply 1. Fastener tilting occurred for configurations in which Ply 1 (e.g., 33 and 43 mils) is lower than 75% of the fastener pitch value (P=62.5 mils, 1.5875mm) and Ply 2 (e.g., 33, 43, 54 and 68 mils) is lower than 125% of P, (i.e. $t_1/P < 0.75$ and $t_2/P < 1.25$). Fastener tilting prediction, in accordance with the fastener pitch, allows to sort test configuration into two groups: “fastener tilting” and “low fastener tilting” group.

For tests within the “fastener tilting” group, the main limit state was tilting and bearing because of local bending deformation occurring at Ply 1. As suggested by the proposed model, local bending deformation at Ply 1 is associated with the moment resisting to the shearing force couple. This resisted moment is a shearing force couple composed of compressive forces due to the fastener head-Ply 1 contact, and of a tensile force traveling through the centerline of the fastener resulted from the thread-Ply 2 contact, which prevent the fastener from pulling out.

Results shown that Ply 2-thread tension and bearing at Ply 2 play an important role of the capacity connection for test included in the “fastener tilting” group. This analysis recommend to combine thread tension and ply bearing capacity to determine the connection capacity. Fastener tilting estimation for each ply configuration should be provided to estimate the weight for each capacity in this combination.

For tests within the “low tilting” group, three limit states were validated according to the proposed model. If Ply 1 was much thicker than Ply 2 (e.g. 9733) the limit state was bearing dominant at Ply 2, leading to fastener bending failure, which was caused by the applying bearing force on the fastener shaft. If Ply 2 was much thicker than Ply 1 (e.g. 4397) the limit state was bearing dominant at Ply 1, leading to fastener shear failure at the head. Finally, if Ply 1 and Ply 2 were quite identical (i.e. 5454, 6843 and 9797) the limit states was a combination of fastener bending and shear.

Finally, this analysis shown that load deformation study from initial load to failure should be considered allows to determine the optimum ply configuration by providing design criteria. The optimum ply combination should be selected into the “fastener tilting” group to prevent fastener from failing in shear or/and bending. Then failure resulting to the tilting and bearing limit state differed for each test. A 33 Ply into a configuration tend to tear because of the

compressive forces (i.e. 3333 and 3368). Therefore, these types of tests are non-desirable. The optimum ply configuration should be taken among the three remaining tests (i.e. 4343, 4354 and 4368) in which Plies allow fastener tilting and support ply bearing demand. For the remaining tests, bearing demand is supported by each ply. For these tests fastener tend to pull out, which caused thread deformation due to tensile force

Table 5-2(Table 5-2). Then, the higher is Ply 2 thickness, the higher is the connection capacity (as long as Ply 2 allows fastener tilting). Therefore, the optimum ply configuration is suggested to be the 4368 tests.

Chapter 6 AISI model in predicted limit states should be reconsidered

Fastener tilting and limit state prediction based on the proposed model has been validated through load deformation study combined with picture analysis for each test. The next step in the analysis model development is to compare and contrast the proposed model with the AISI model in predicted limit states. The AISI limit states are tilting, tilting and bearing, and bearing selected according to the ratio t_2 over t_1.

6.1 AISI model compare to the proposed model in predicting fastener limit states

Limit states predictions for the AISI model and for the proposed model are compared with tests results in Table 6-1. Results show the inconsistencies in the AISI model in predicting the connection limit states and show the accuracy of the proposed model. A visual comparison through a contour map between the AISI (Figure 6-1) and the proposed model (Figure 6-2) in predicted limit states are provided. The figures highlight the limit states as a function of Ply 1 and Ply 2, ply thicknesses ranging from 33 to 97 mils.

Table 6-1 Comparison between the proposed model and AISI model with experimental results.

Tests	P_{ns} (N)	Limit State Predictions to the Results			
		AISI	AISI	Results	MODEL
3333	2806	T	×	T/B	✓
4343	4924	T	×	T/B	✓
4354	5502	T+B	✓	T/B	✓
4368	6419	T+B	✓	T/B	✓
3368	6321	T+B	✓	T/B	✓
5454	6063	T	×	Bending/shear	✓
6843	6387	T	×	Bending/shear	✓
9797	6524	Shear	×	Bending/shear	✓
9733	4219	T	×	Bearing dom. Ply2	✓
4397	7761	T+B	×	bearing dom. Ply1	✓

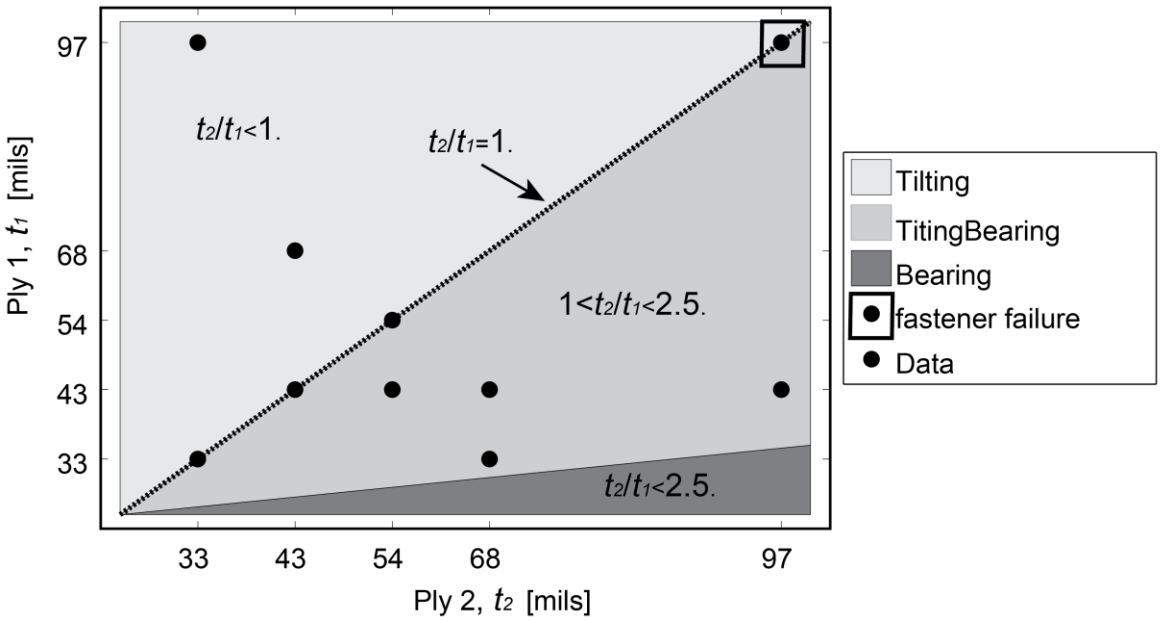

Figure 6-1 AISI model in predicted limit states using thickness ratio t_2/t_1

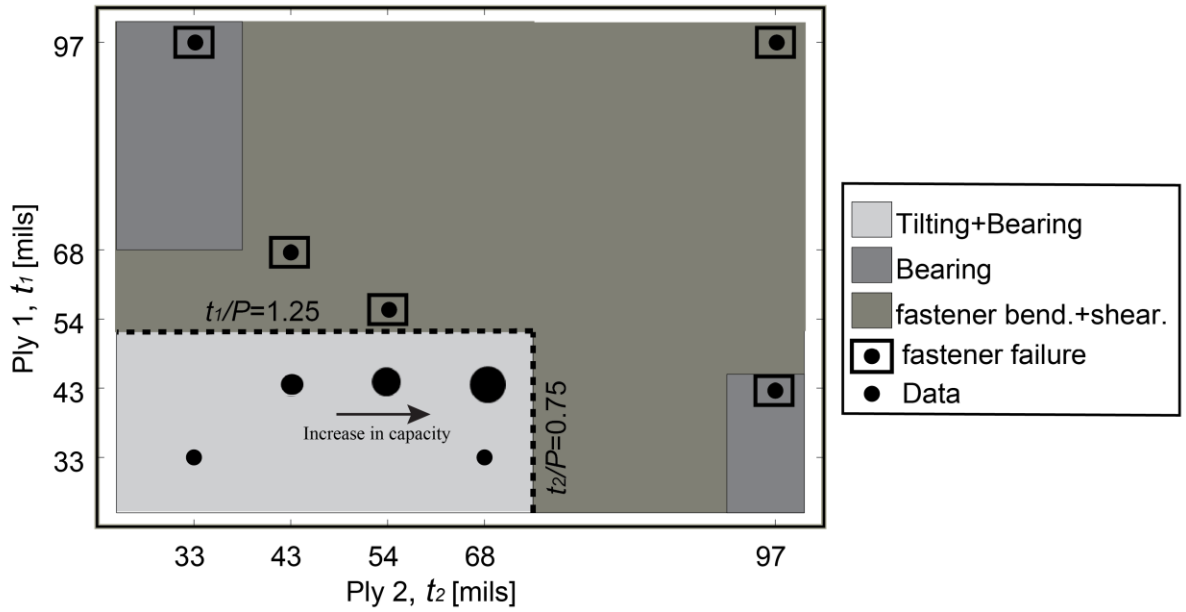

Figure 6-2 Proposed model in predicted limit states using ply thickness over fastener pitch, t1/P and t2/P

The visual comparison of the two models (Figure 6-1, Figure 6-2) highlights that both models differ in predicting fastener tilting and limit states in multitude ways.

First, the AISI model fails in predicting bending and/or shear fastener failure. The AISI model predicted tilting, or tilting and bearing for ply configurations predicted to be in the "low tilting group" by the proposed model (i.e. 9733, 5454, 6843 and 4397) The AISI prediction was incorrect since all the tests failed in fastener bending and/or shear. AISI model predicted only one ply configuration to fail because of the fastener, while five ply configurations failed in this mode as predicted by the proposed model.

Second, the AISI model predicts tilting for thick Ply 1 connected with a thin Ply 2 (e.g., 9733) while the proposed model predicts low tilting for this configuration. Results validated the proposed model because the head-Ply 1-thread contact prevented the fastener from rotating.

The previous analysis in comparing AISI and the proposed model was based on the mean value for each test. This section compares the two models bases on the ratio of the capacity values for all tests and the AISI capacity equations selected based on the predicted limit state for each model (Table 6-2). For tests into the " fastener tilting group" of the proposed model , AISI tilting equation is selected to predict the capacity for each test of this group, except for the 3368 test where bearing at Ply 1 is selected . For tests that were predicted to fail in fastener shear and bending (i.e. 5454, 6843, 9797), the 9797 mean capacity test is selected as the predicted value. For two remaining tests (i.e 9733 and 4397) bearing AISI equation at the thinnest ply is selected. Results show that the mean value of the ratio $P_{ns}test/P_{ns}AISI$ for all tests is 0.83 with a coefficient of variation of 0.24 while the ratio $P_{ns}test/P_{ns}model$ for all tests is 0.90 with a coefficient of variation of 0.17.

Table 6-2 Numerical AISI prediction vs Model prediction and Results

						AISI								μ	cυ		μ	cυ
Specimen	t_1 [mm]	t_2 [mm]	t_2/t_1	Fu_1 [Mpa]	Fu_2 [Mpa]	Tilting [N]	Bearing Ply 1 [N]	Bearing Ply 2 [N]	Shear [N]	$P_{ns}AISI$ [N]	$P_{ns}model$ [N]	$P_{ns}test$ [N]	$P_{ns}test/P_{ns}AISI$	$P_{ns}test/P_{ns}AISI$	$P_{ns}test/P_{ns}AISI$	$P_{ns}test/P_{ns}model$	$P_{ns}test/P_{ns}model$	$P_{ns}test/P_{ns}model$
3333-1	0.87	0.87	1.00	444	64.45	3332	5042	5042	8162	3332	3332	2614	0.78			0.78		
3333-2	0.87	0.87	1.00	444	64.45	3332	5042	5042	8162	3332	3332	3031	0.91	0.83	0.09	0.91	0.83	0.09
3333-3	0.87	0.87	1.00	444	64.45	3332	5042	5042	8162	3332	3332	3014	0.90			0.90		
4343-1	1.19	1.19	1.00	456	456	5448	7059	7059	8162	5448	5448	4824	0.89			0.89		
4343-2	1.19	1.19	1.00	456	456	5448	7059	7059	8162	5448	5448	5047	0.93	0.90	0.02	0.93	0.90	0.02
4343-3	1.19	1.19	1.00	455	455	5444	7051	7051	8162	5444	5444	4850	0.89			0.89		
9733-1	2.54	0.87	0.34	532	445	3319	17640	5032	8162	3319	5032	4290	1.29			0.85		
9733-2	2.54	0.87	0.34	532	445	3319	17640	5032	8162	3319	5032	3612	1.09	1.20	0.07	0.72	0.79	0.07
9733-3	2.54	0.87	0.34	532	445	3319	17640	5032	8162	3319	5032	4032	1.21			0.80		
5454-1	1.41	1.41	1.00	533	533	8200	9765	9765	8162	8162	6677	6324	0.77			0.95		
5454-2	1.41	1.41	1.00	533	533	8200	9765	9765	8162	8162	6677	6274	0.77	0.75	0.03	0.94	0.92	0.03
5454-3	1.41	1.41	1.00	533	533	8200	9765	9765	8162	8162	6677	5886	0.72			0.88		
6843-1	1.81	1.19	0.66	496	456	5443	11719	7055	8162	5443	6677	5223	0.96			0.78		
6843-2	1.81	1.19	0.66	496	456	5443	11719	7055	8162	5443	6677	6102	1.12	1.11	0.11	0.91	0.91	0.11
6843-3	1.81	1.19	0.66	496	456	5443	11719	7055	8162	5443	6677	6810	1.25			1.02		
4354-1	1.19	1.40	1.18	456	531	8132	7055	9699	8162	7593	8132	5457	0.72			0.67		
4354-2	1.19	1.40	1.18	456	531	8132	7055	9699	8162	7593	8132	5440	0.72	0.73	0.02	0.67	0.69	0.02
4354-3	1.19	1.40	1.18	456	531	8132	7055	9699	8162	7593	8132	5683	0.75			0.70		
4354-4	1.19	1.40	1.18	456	531	8132	7055	9699	8162	7593	8132	5709	0.75			0.70		
3368-1	0.88	1.81	2.05	444	496	11169	5113	11719	8162	8141	5113	5943	0.73			1.16		
3368-2	0.88	1.81	2.05	444	496	11169	5113	11719	8162	8141	5113	6824	0.84	0.68	0.23	1.33	1.08	0.23
3368-3	0.88	1.81	2.05	444	496	11169	5113	11719	8162	8141	5113	3815	0.47			0.75		
4368-1	1.19	1.83	1.54	456	492	11230	7055	11729	8162	9142	7055	6343	0.69			0.90		
4368-2	1.19	1.83	1.54	456	492	11230	7055	11729	8162	9142	7055	6013	0.66	0.69	0.03	0.85	0.89	0.03
4368-3	1.19	1.83	1.54	456	492	11230	7055	11729	8162	9142	7055	6494	0.71			0.92		
4397-1	1.19	2.55	2.15	456	524	19666	7055	17397	8162	13361	7055	7802	0.58			1.11		
4397-2	1.19	2.55	2.15	456	524	19666	7055	17397	8162	13361	7055	8465	0.63	0.57	0.10	1.20	1.08	0.10
4397-3	1.19	2.55	2.15	456	524	19666	7055	17397	8162	13361	7055	6601	0.49			0.94		
9797-1	2.55	2.55	1.00	523	523	19687	17400	17400	8162	8162	6677	7139	0.87	0.82	0.07	1.07	1.00	0.07
9797-2	2.55	2.55	1.00	523	523	19687	17400	17400	8162	8162	6677	6215	0.76			0.93		
												μ_1	**0.83**		**μ_2**	**0.90**		
												$c_{\upsilon 1}$	**0.24**		**$c_{\upsilon 2}$**	**0.17**		

Therefore, results from Table 6-2 demonstrate that the proposed model is more accurate to predict limit states than the AISI model as the proposed model uses the AISI predicted capacity equations in more appropriate and accurate way. For example, bearing at Ply 1 was well observed as the 97 Ply 2 prevented the fastener to tilt. The proposed model predicts correctly the connection capacity for this test as the ratio $P_{ns}test/P_{ns}model$ is equal to 1.08 (mean value of the three tests), where $P_{ns}model$ is the AISI bearing equation at Ply 1. While, the ratio $P_{ns}test/P_{ns}AISI$ is equal to 0.57. The ratio is low because AISI model takes a linear combination between the tilting and bearing AISI capacity equation when the ratio $1< t_2/t_1.<2.5$.

The reason that both models differ in predicting limit states comes from the incorrect use of design parameters to predict limit states. AISI model predict limit states according to the thickness ratio t_2/t_1. This can be interpreted as a 3333 ply configuration would have the same tilting limit state as a 5454 ply configuration ($t_2/t_1=1$). Results show these two ply configurations differ considerably in their behavior. AISI predicts a titling limit state for the 5454 tests as do 3333 tests, although it was observed to fail based on a combination of shear and bending of the screw.

The proposed model suggests to reconsider the use of design parameter such as ply thickness and suggests to include the fastener pitch. Fastener pitch differs as a function of the fastener diameter, the higher is the fastener diameter the highest is the pitch, thus fastener diameter is not considered. The use of the ratio of the each ply over the fastener pitch comes from the suggestion of the proposed model to consider the fastened connection as a combination of the head-Ply1-thread contact with thread-Ply2-thread contact. This combination allowed the proposed model to predict fastener tilting and limit states correctly.

The proposed model uses design parameters to estimate fastener tilting, while AISI model combines design parameters (i.e. ratio t_2/t_1) and capacity equations to predict limit states. If $t_2/t_1<1$ the lower predicted capacity among the tilting and bearing equations predicts the corresponding limit state. The next section shows that the tilting equation always provides the lowest capacity, thus tilting is always predicted for $t_2/t_1<1$.

6.2 AISI tilting equation should be ameliorated to predict tilting and bearing limit state

The analysis of this section focus on the AISI capacity equations to demonstrate few contradictions in these equations in predicting limit states.

First, the contradiction in the AISI tilting Equation (Eq 6.1) results in the consideration of Ply 2 only in predicted tilting limit state. This is contradictory to the results as the analysis validated Ply 1 guides fastener tilting.

$$P_{ns} = 4.2\sqrt{t_2^3 d}\,Fu_2 \qquad \text{Eq. 6.1}$$

Second, AISI tilting limit state is always predicted in the case of ply configuration being $t_2/t_1\leq 1.0$ while AISI suggests bearing limit state may occur instead of tilting. For the case where Ply 2 is thinner than Ply 1, the AISI capacity equations predict limit state according to the minimum capacity P_{ns} among the tilting (Eq. 1) and bearing equations (Eq. 6.2 and 6.3). Among the two bearing equations, the thinner is the ply the lower is the capacity. Therefore bearing at Ply 1 cannot be predicted and bearing equation at Ply 1 (Eq. 3) can be denied.

$$P_{ns} = 2.7 t_2 d Fu_2 \qquad \text{Eq. 6.2}$$

$$P_{ns} = 2.7 t_1 d Fu_1 \qquad \text{Eq. 6.3}$$

To determine the lowest predicted capacity between the tilting equation (Eq. 6.1) and bearing at Ply 2 equation (Eq. 6.2), the analysis graphs both equations in which P_{ns}/Fu_2 is in a function of t_2. Fu_2 is set to the unit value 1.The first graphs (Figure 6-3) determines tilting and bearing P_{ns} as a function of t_2 (range from 33 to 97 ply) for a fastener diameter d of 0.19 in (4.826 mm, Hex #10). The second graphs (Figure 6-4) determines tilting and bearing P_{ns} as a function of t_2 for a fastener diameter d of 0.165 in (4.191 mm, Hex #08). In both figures, the AISI tilting equation is represented by dashed line while the AISI bearing equations is represented by line. The lowest curve among the two curves predict the corresponding limit state.

The analysis of the first graphs determines that tilting limit state is always predicted for a Ply 2 with thickness range from 33 to 97 mils and a Hex #10 fastener. The tilting curve is lower than the bearing curve at this Ply 2 range. This prediction is contradictory to the results since it was analyzed by the proposed model that a test such as 9733 (Ply 1: 97 ; Ply 2: 33) should not tilt while AISI equation predicts fastener tilting. This contradiction shows again the AISI model limit by only including t_2 in the AISI tilting equation.

Furthermore, the analysis of the second graphs determines that the fastener diameter plays a controversial role in the AISI's tilting equation. Indeed, both tilting and bearing equations are related to the fastener diameter d. By comparing the curves from both figures, the largest fastener diameter is predicted to tilt for a larger range of t_2. Indeed, the intersection point between the tilting and bearing curves appears at a t_2 value of 78 mils when using a #10 Hex screw, while this intersection appears at 68 mils for a #08 Hex screw. Thus, the tilting limit state is predicted for Ply 2 thickness in range from 33 to 78 for a #10 Hex screw, while tilting is predicted for Ply 2

thickness in range from 33 to 68 for a #08 Hex screw. This is inconsistent with the proposed model since larger fastener diameter should tend to bear the ply rather than tilt.

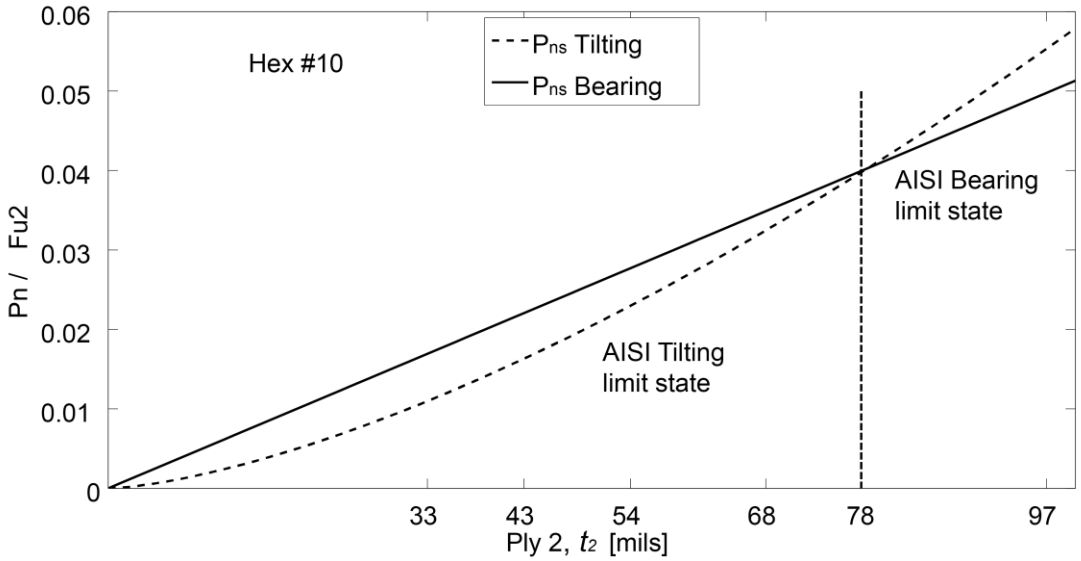

Figure 6-3 Pns /Fu function of Ply 2 thickness t_2 for diameter values d=0.19’’(Hex #10).The lowest curve provides the predicted AISI limit state in the case t_2/t_1 <1

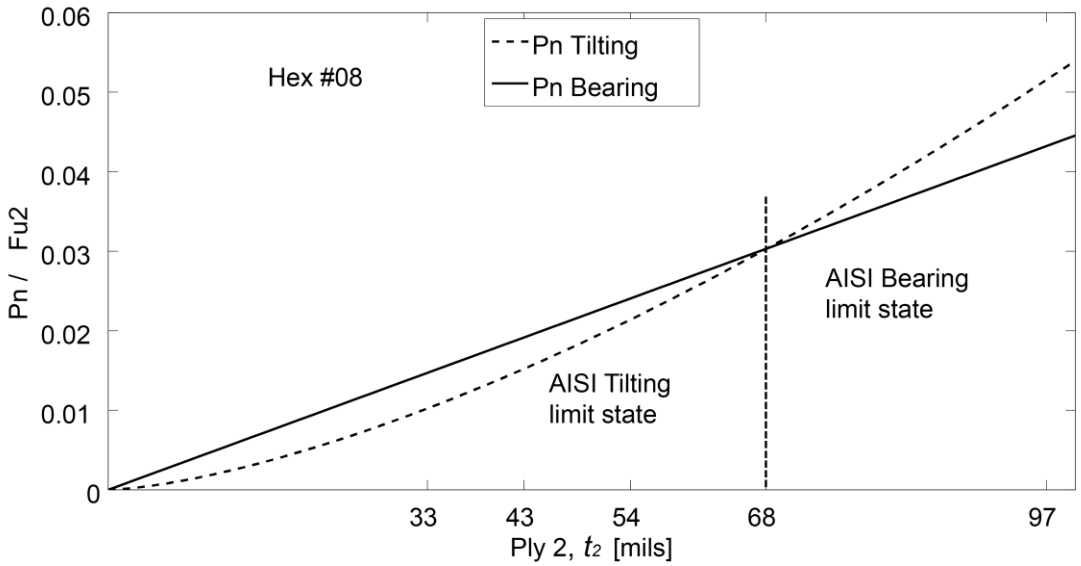

Figure 6-4 Pns /Fu function of Ply 2 thickness t_2 for diameter values d=0.165’’(Hex #08). The lowest curve provides the predicted AISI limit state in the case t_2/t_1 <1

Finally, AISI model does not predict bearing at Ply 2 for any case scenario because AISI model predicts fastener tilting for the condition $t_2/t_1 \leq 1.0$ and predicts tilting and/or bearing at Ply 1 for $1 \leq t_2/t_1$ since Ply 1 would be thinner than Ply 2. This is contradictory with the analysis of the results as bearing at Ply 2 was observed for the 9733 test.

The last analysis of this research proposes a shift in the methodology to predict connection limit states. The proposed model suggests to predict limit states based on design parameter such as ply thicknesses and faster pitch rather than identifying limit states by capacity equations. Identifying the limit state of a connection when two ply configuration have equivalent peak values becomes a challenge. For example, study of the 4368 and 6843 test shown that both tests have equivalent P_{ns} value, P_{ns} = 6387 N for the 6843 test and the P_{ns} = 6419 N for the 4368 test,

While both tests differs in their limit states. The 6843 test fail in shear and bending of the fastener while the 4368 test has a bearing and tilting limit state. Therefore, the analysis suggests to use the limit states study to predict capacity equation. An understanding of the connection behavior should lead to more precision in using current capacity equation or create new ones.

Chapter 7 Conclusion

A study of screw-fastened cold-formed steel-to-steel shear connections was investigated in the research described in this thesis. A proposed model was suggested to improve the current limit states of the AISI model. The proposed model was validated by an experimental test study, in which results were used to correlate the deformation occurring at the connection to the load-deformation response. Thus, this study provided new evidence for a revision to current limit states.

Results suggest that fastener tilting plays a key kinematics in the limit state prediction and that test configurations need to be sorted according to fastener tilting prediction. Results confirmed that the screw fastener pitch value should be considered as a design factor in predicting fastener tilting. Fastener tilting is predicted if Ply 1 is lower than 75% of the fastener pitch and if Ply 2 is lower than 125 % of the fastener pitch. In configurations that are outside these boundaries, the fastener failed in shear, bending, or combined shear and bending.

The analysis determined the optimized ply configuration into the “tilting” group. Ply 1 should be taken to allow fastener tilting and prevent tearing due to local bending of the ply causing by local bending deformation. Using a Hex #10 fastener, a 43 Ply 1 was the best match for this design recommendation. On the other hand, Ply 2 should be taken to allow fastener tilting and to prevent pull out of the fastener by tension of the threads with Ply 2. A 54 and 68 Ply 2 were the best match for this recommendation. The 68 Ply 2 provided higher capacity because of Ply 2 deflection and material hardening around the fastener during load softening.

This optimum results and study of load deformation for each curves should allow future studies in cyclic load deformation to select test where connection behaviors are not desirable

such as fastener failure or ply tearing. In addition, results show that Ply 2 increased capacity of the connection for test experiencing tilting and that Ply 1 should guide stiffness of the connection for the same tests since Ply 1 governs fastener rotation.

The analysis also determined that AISI model in predicting limit states was inaccurate. The reasons for this inaccuracy is because AISI tilting equation does not take Ply 1 into account in the equation, while the analysis determined that Ply 1 guides fastener tilting. Then bearing at Ply 2 is not predicted for any scenario. The proposed model suggests to review the limit states prediction by considering ply thickness over fastener pitch instead of the ratio Ply 2 over Ply 1.

Better results could have been provided about these deformations (i.e. hole elongation measurement, ply displacement, ply deflection). For future research focusing on limit state, this research suggests improvement of the self-made optical device. Precision was lost because the wooden rod deteriorated after test repetitions. The length of the rod is a sensitive value in measuring fastener and ply displacement, thus, a plastic rod is suggested instead of wood. The same suggestion applies to the circular targets that affix wooden rod to the plies. These targets tend to bend after several testing runs which reduces the quality of the measurement. Moreover, precision in the results were diminished because, at times, the test set up shifted to few degrees during testing. The optical measurement allowed shifts to be observed, which were excluded from the dataset. To address this issue, connection at the test set-up should be welded instead of using large screws. All these modifications will provide better results especially if stiffness and capacity equations are studied.

Future research should focus on predicted peak load and initial stiffness according to the detailed limit states provided in this research. All these deformations at each ply and at the fastener need to be taken into account for capacity equations based on configurations defined by "tilting" groups.

References

AISI (2012). "North American specification for the design of cold-formed steel structural members." Section E.4.3, American Iron and Steel Institute, Washington , D.C.

AISI (1999). "AISI Statistical Highlights Of The North American Steel Industry", American Iron and Steel Institute.

ASTM (2008), ASTM E8/E8M-08: Standard test methods for tension testing of metallic materials

BSI (1987). "British Standard - Structural Use of Steelwork in Building - Part 5. Code of Practice for Design of Cold-Formed Sections."

Casafont, M., Arnedo, A., Roure, F., and Rodrıguez-Ferran, A. (2006). "Experimental testing of joints for seismic design of lightweight structures. Part 1. Screwed joints in straps." Thin-Walled Structures, 44(2), 197–210.

Daudet, L., and LaBoube, R. (1996). "Shear behavior of self drilling screws used in low ductility steel." Proc., 13th International Specialty Conference on Cold-Formed Steel Structures, University of Missouri-Rolla, 595–613.

ECCS (1987). "European Recommendations for the Design of Light Gage Steel Members". Brussels, Belgium.

Francka, R. M., and LaBoube, R. A. (2009). "Screwed connection subject to tension pull-out and shear forces."

Haus, A. (2014). Energy Dissipation of Cold-Formed Steel Connections. Virginia Tech Structural and Engineering Materials Report No. CE/VPI-ST-14/02, Blacksburg, Virginia.

Hendawi, S., and Frangopol, D. M. (1994). "System reliability and redundancy in structural design and evaluation." Structural Safety, 16(1), 47-71.

Laboube, R. A., and Sokol, M. A. (2002). "Behavior of screw connections in residential construction." Journal of Structural Engineering, 128(1), 115–118.

Leng, J., Schafer, B. W., and Buonopane, S. G. (2012). "Modeling the seismic response of cold-formed steel framed buildings: model development for the CFS-NEES building." Annual Stability Conference - Structural Stability Research Council, St. Louis, Missouri.

Lim, J., and Nethercot, D. (2004). "Stiffness prediction for bolted moment-connections between cold-formed steel members." Journal of Constructional Steel Research, 60(1), 85–107.

Merwe, P. v. d. (1987). "Development of design criteria for ferritic stainless steel cold-formed structural members and connections " Ph.D. thesis, University of Missouri-Rolla.

C.D. Moen, D. A., Padilla-Llano, S. Corner, C. Ding (2014). "Towards Load-Deformation Models for Screw-Fastened Cold-. Formed Steel-to-Steel Shear Connections", Conference on Cold-formed Steel Structures, Missouri S&T, St. Louis, Missouri, U.S.A.

Peköz, T. (1990). "Design of cold-formed steel screwed connections." Tenth International Specialty Conference on Cold-formed Steel Structures, Missouri S&T, St. Louis, Missouri, U.S.A.

Serrette, R., and Peyton, D. (2009). "Strength of screw connections in cold-formed steel construction." Journal of Structural Engineering, 135(8), 951–958.

StructSoft Solution (2014), www.strucsoftsolutions.com, website

Uang, C., and Sato, A. (2010). "Cyclic Testing and Modeling of Cold-Formed Steel Special Bolted Moment Frame Connections." Journal of Structural Engineering, 136(8), 953–960.

Winter, G. (1956). "Tests on bolted connections in light gage steel." Proceedings of the American Society of Civil Engineers, 101(7), 1381-1391.

Zadanfarrokh, F., and Bryan, E. (1992). "Testing and design of bolted connections in cold-formed steel sections." Eleventh international specialty conference on cold-formed steel structures University of Missouri-Rolla, St. Louis, Missouri, U.S.A.

Zaharia, R., and Dubina, D. (2006). "Stiffness of joints in bolted connected cold-formed steel trusses." Journal of Constructional Steel Research, 62(3), 240–249.

Appendix A Stiffness fit lines on load deformation response using statistic toolbox

Two methods are used to determine the initial slope of a curve, the tangent stiffness or the secant stiffness. The secant stiffness – slope value between any point of the curve and the initial point, differs from the tangent stiffness being the local slope at a selected point. While a linear load deformation causes the secant and tangent stiffness to be identical and consistent with initial stiffness, the nonlinear load deformation causes the secant stiffness values to greatly drop making the computation of an initial stiffness difficult. For example, the 4343 configuration (Figure -A-1) exhibits decreased secant stiffness from 2.3 to 0.6 10^{4}N/mm during a short 0.5 mm crosshead displacement, leading to the question, *"Which secant stiffness value should be selected as the load deformation initial stiffness on such wide range of possible values?"*.

Indeed, any value on the secant stiffness range can be set as initial stiffness. Some researchers would intend to pick the first value corresponding to the stiffness at an instantaneous first displacement while others would suggest to select the secant stiffness value that intercepts 0.4 times the first maximum peak load.

To answer this question a custom analysis, based on the standardized normal curve using Z score $Z=(x-\mu)/\sigma$, is proposed to estimate the initial stiffness of the load deformation. Where x is the secant stiffness values, μ is the mean of the secant stiffness values; σ is the standard of deviation of secant stiffness values.

Secant stiffness values are computed up to and beyond the first maximum peak load after softening. The decreased secant stiffness results from the combined fastener/ply stiffness degradation as the connection progresses through load-deformation, Figure -A-1.

The distributed secant stiffness data is shown on Figure -A-2. The positive and negative

Z values represent the highest and lowest secant stiffness values respectively. Usually, a Z value of 2 is taken to select 95% of the data, meaning that data lie within 2 standards of deviations of the mean. The non-normalized distributed secant stiffness conducts to review this value and an empirical value of 80% of Zmax is suggested. Secant stiffness data values from 80% of Zmax to Zmax are selected to determine the initial stiffness on the load deformation curve, by generating a regression line on that data. The selected data is displayed in blue on Figure -A-1, 2 and3.

The second stiffness line is generated using a regression line on data lying between +/- 0.5 standard of deviation from the mean. Secant stiffness data values from Zmin to 80% of Zmin are selected to determine the third stiffness line.

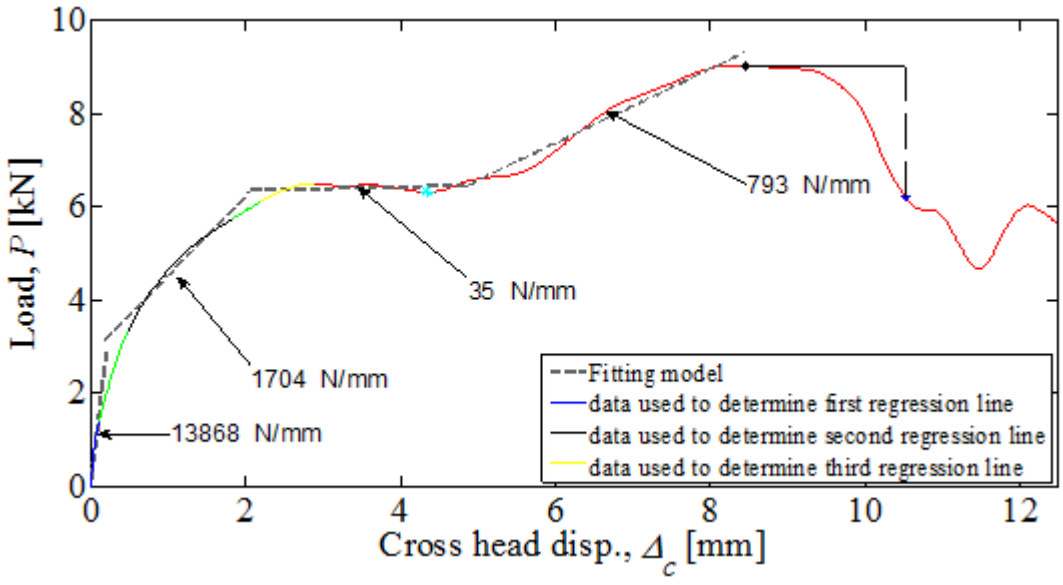

Figure -A-1 Load deformation curve for a 4368 test including stiffness degradation lines with their respective stiffness values.

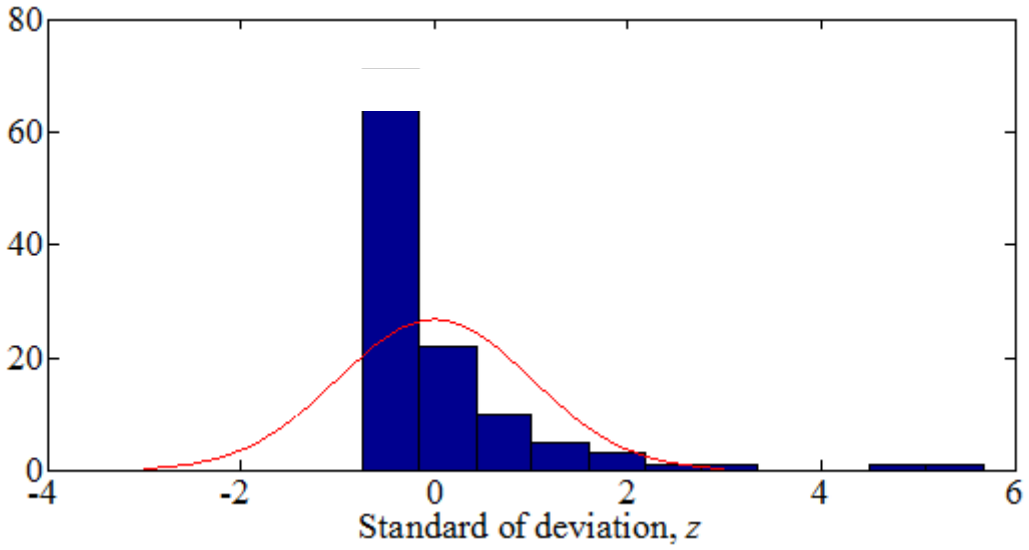

Figure -A-2 Secant stiffness distribution comparing to a normal distribution for the 4368 test

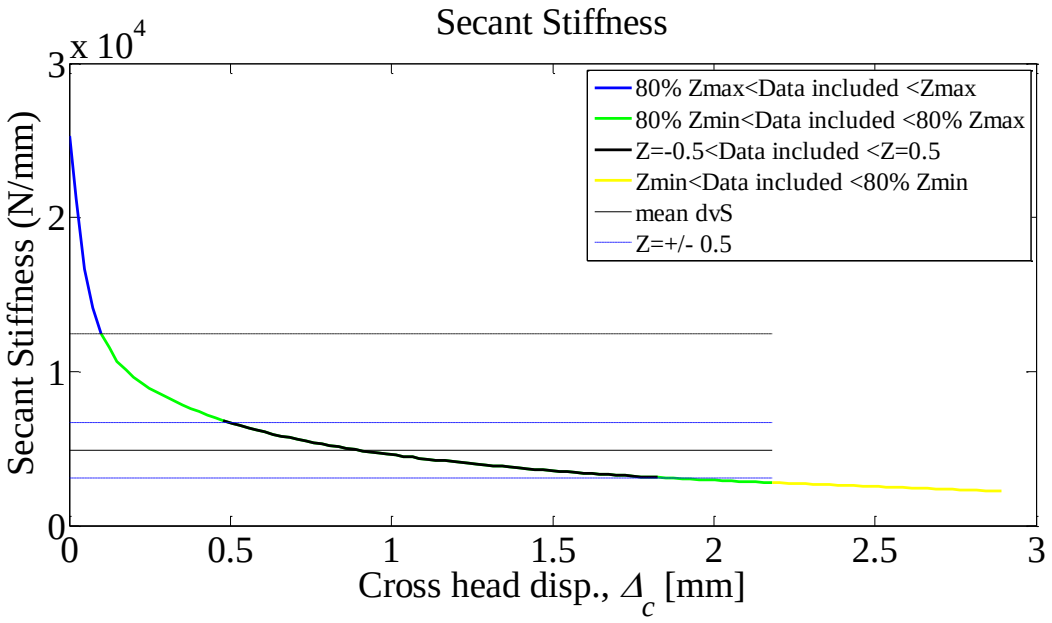

Figure -A-3 Secant stiffness values as a function of the cross head disp. for the 4368 test.

Appendix B Load deformation curves for each ply configuration

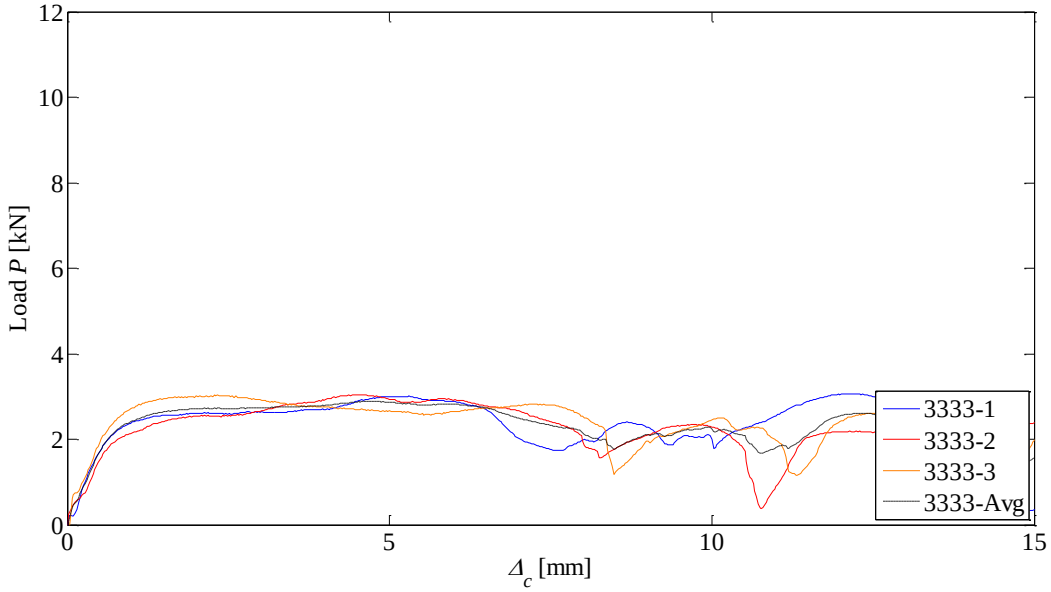

Figure -B-1 Average Load curves for 3333 test

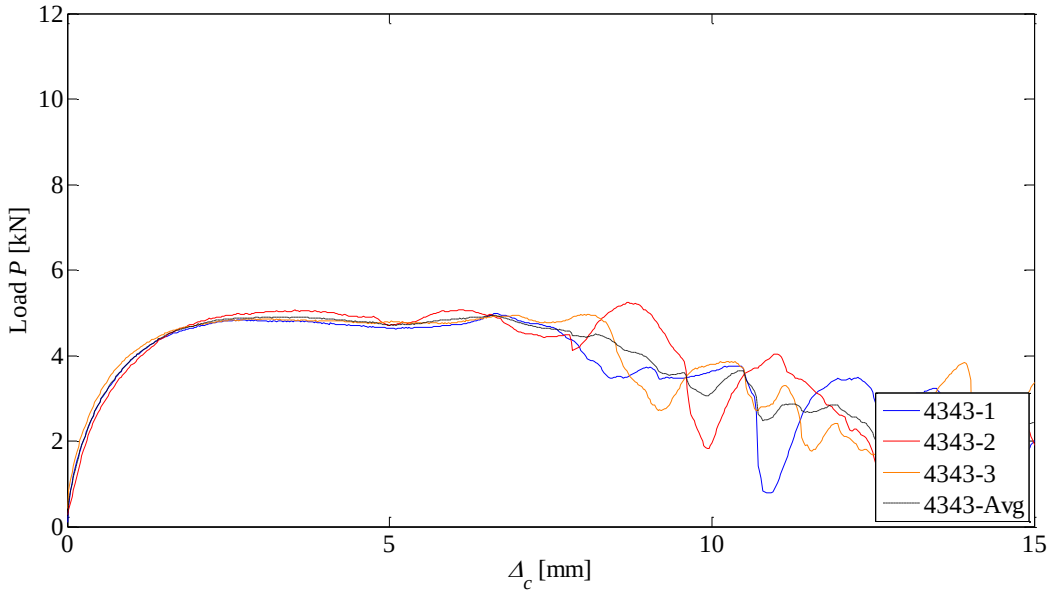

Figure -B-2 Average Load curves for 4343 test

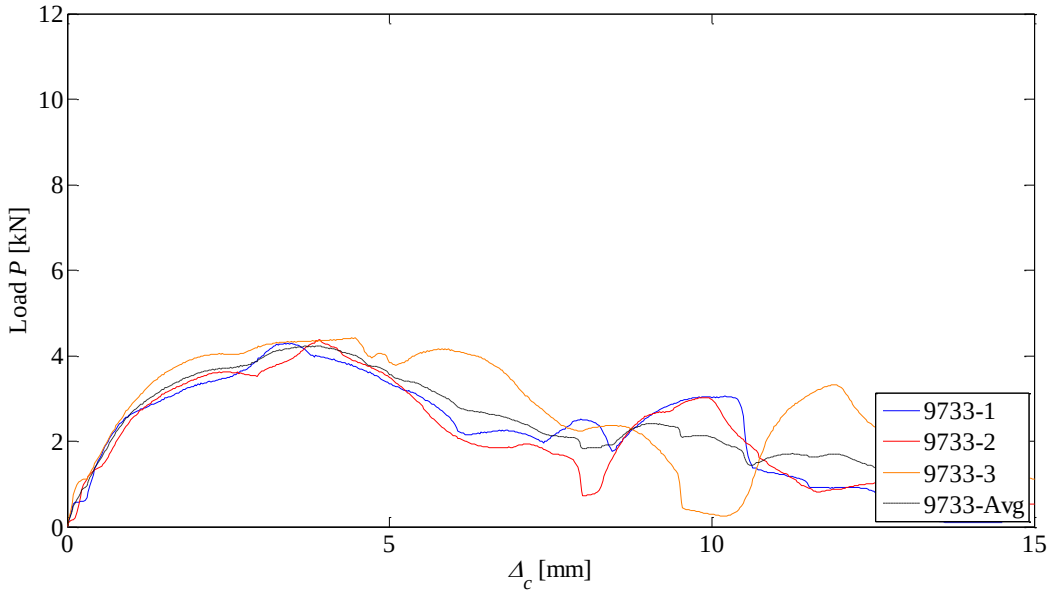

Figure -B-3 Average Load curves for 9733 test

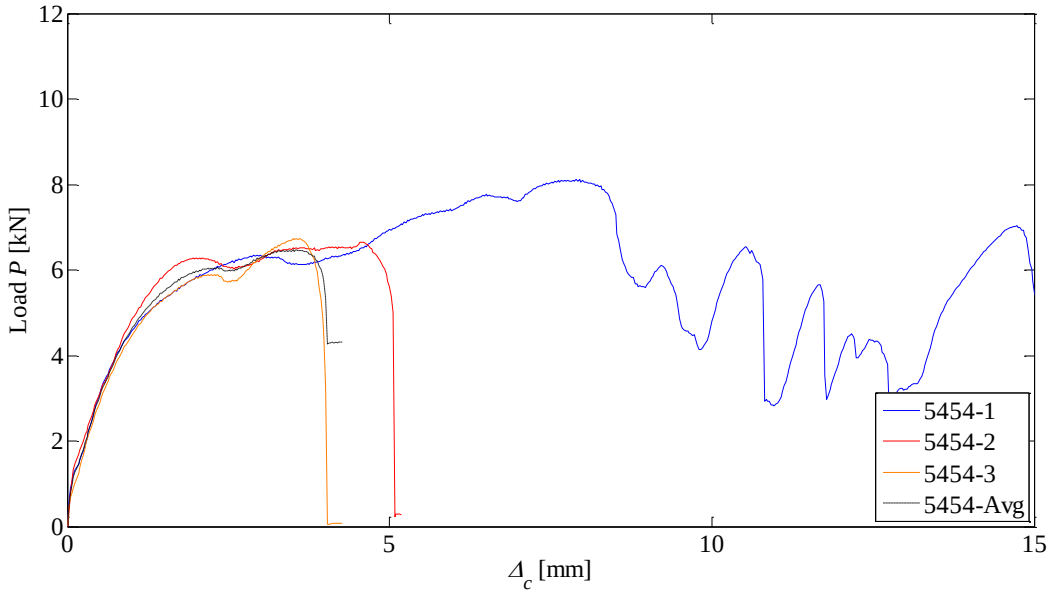

Figure -B-4 Average Load curves for 5454 test

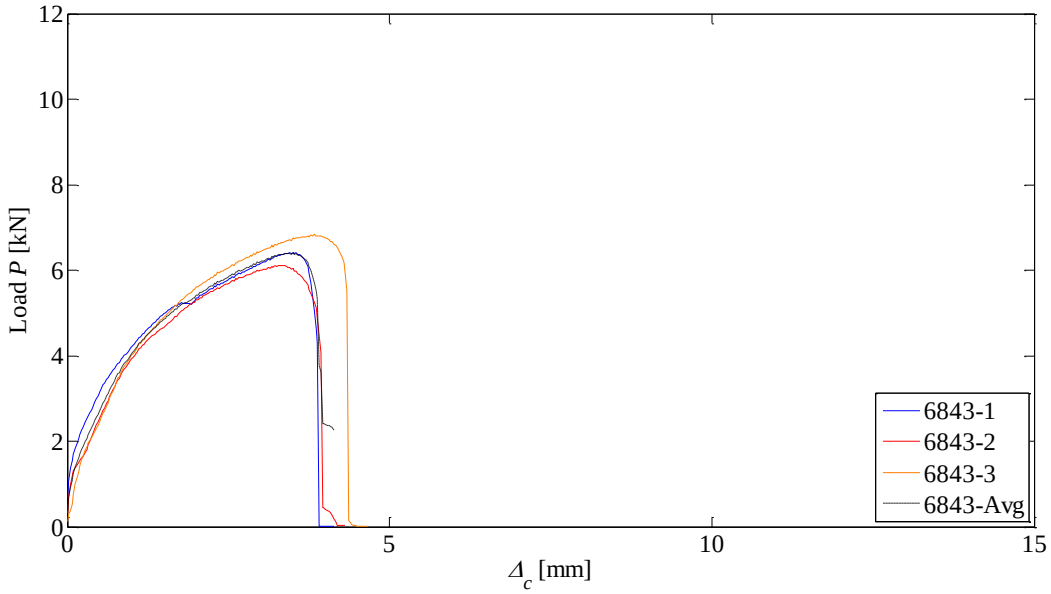

Figure -B-5 Average Load curves for 6843 test

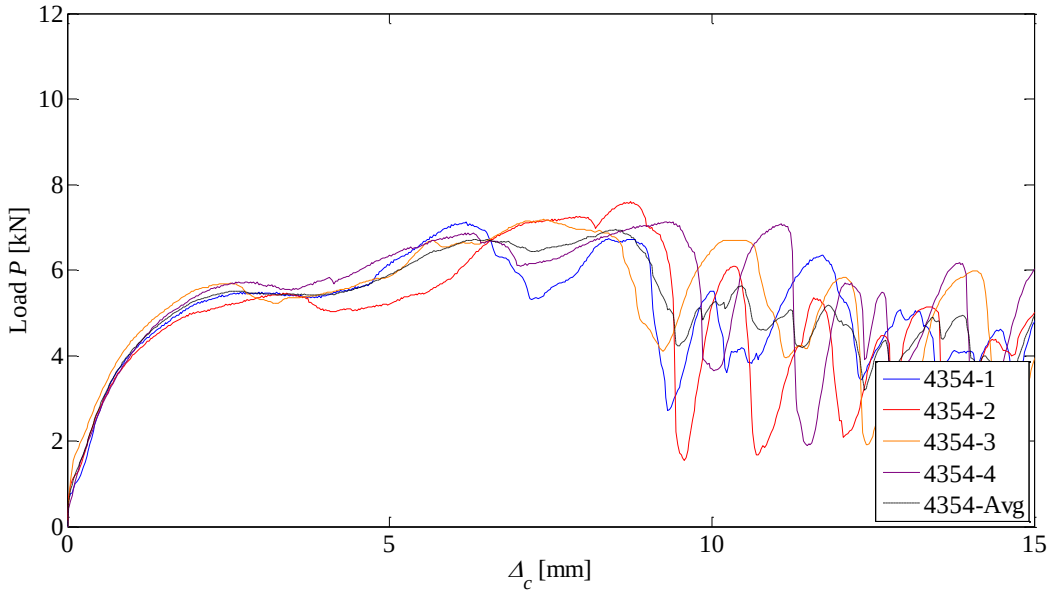

Figure -B-6 Average Load curves for 4354 test

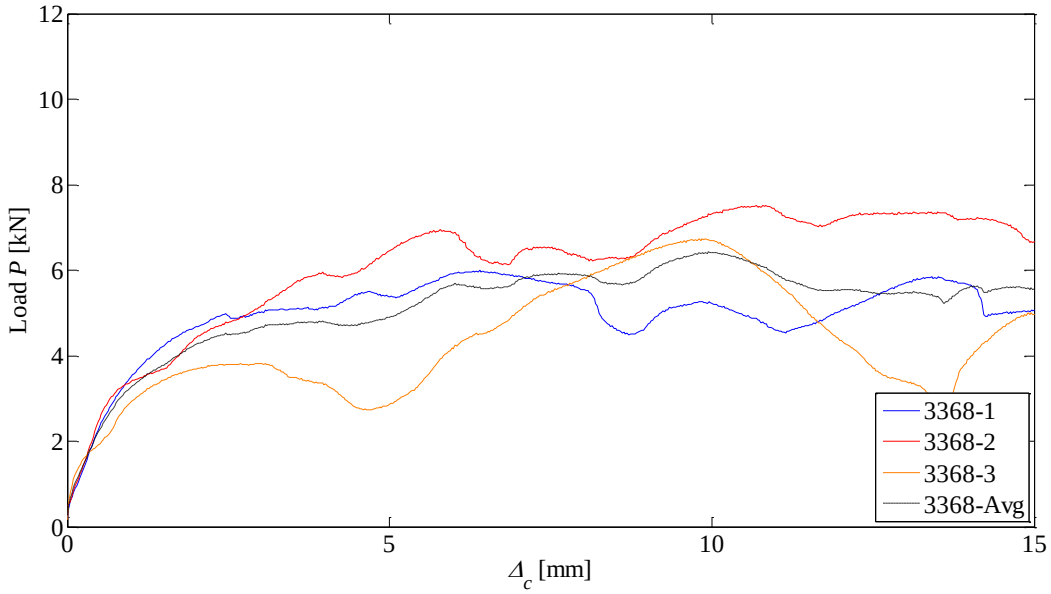

Figure -B-7 Average Load curves for 3368 test

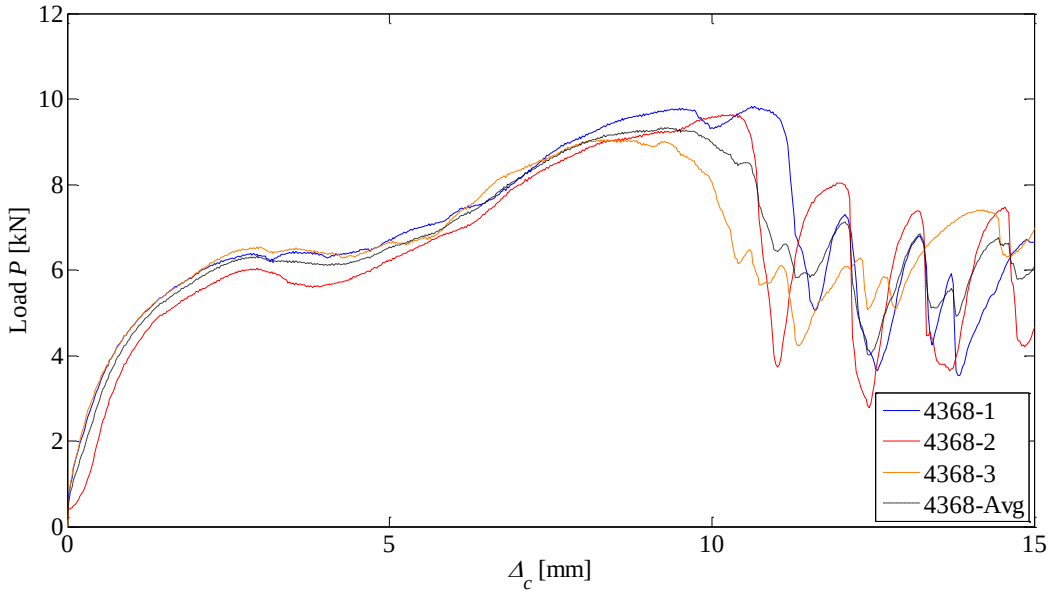

Figure -B-8 Average Load curves for 4368 test

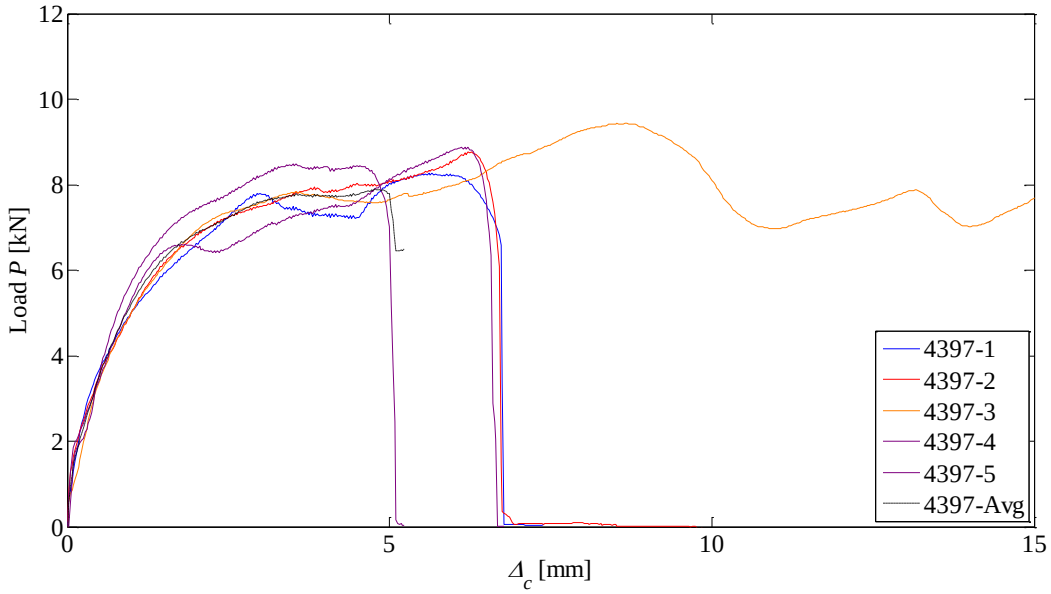

Figure -B-9 Average Load curves for 4397 test

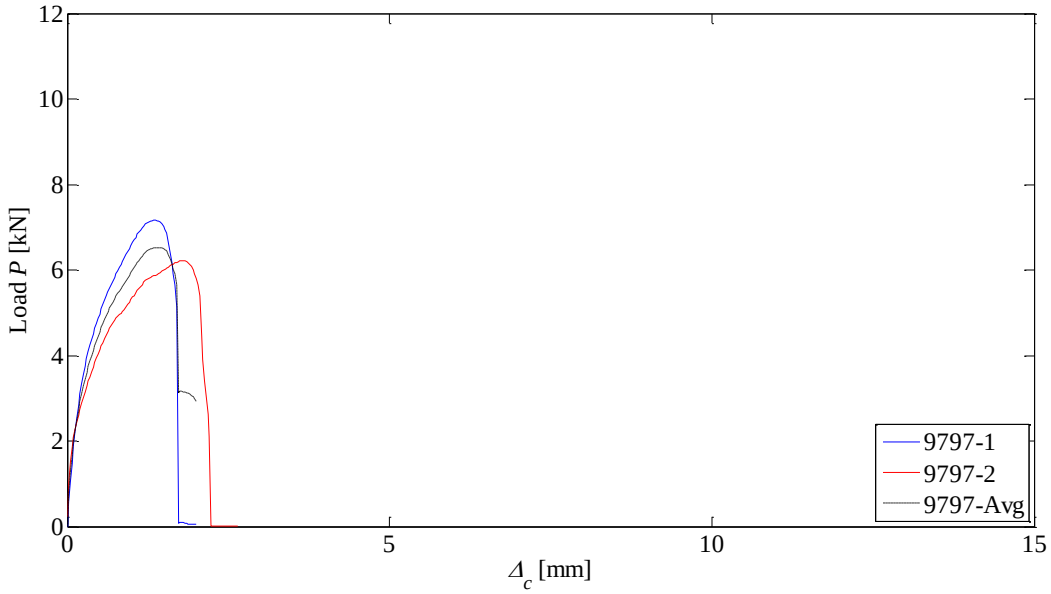

Figure -B-10 Average Load curves for 9797 test